AD-A130 765 SYNTHETIC SEISMOGRAM CALCULATIONS FOR TWO-DIMENSIONAL VELOCITY MODELS(U) PURDUE UNIV LAFAYETTE IN DEPT OF GEOSCIENCES L W BRAILE ET AL. 20 MAY 83 TR-1-83-ONR 1/1

UNCLASSIFIED N00014-82-K-0033 F/G 8/11 NL

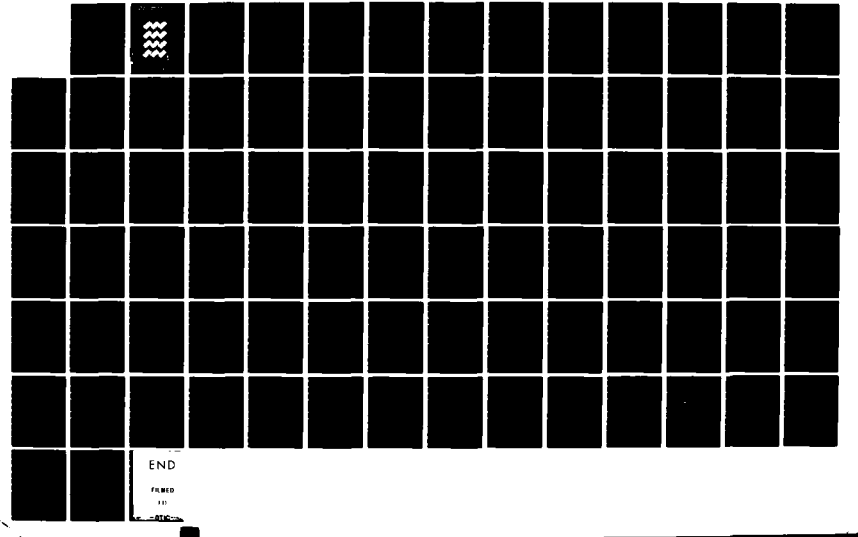

END

FILMED

DTIC

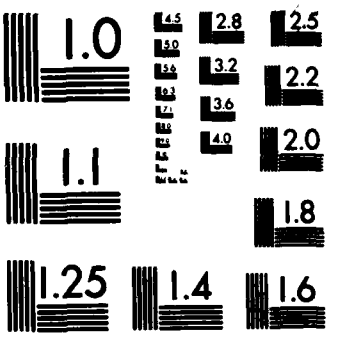


MICROCOPY RESOLUTION TEST CHART
NATIONAL BUREAU OF STANDARDS-1963-A

AD A130765

(12)

DTIC
ELE
JUL 26 1983
S
A

Contract No. DNR-1-83
Office of Naval Research
N00014-82-K-0083
07 26 003
3/1/83 to 3/30/83
6/20/83

Department of Geosciences
PURDUE UNIVERSITY

Final Technical Report

for the

OFFICE OF NAVAL RESEARCH
Contract No. N00014-82-K-0033

# SYNTHETIC SEISMOGRAM CALCULATIONS FOR TWO-DIMENSIONAL VELOCITY MODELS

by

Lawrence W. Braile, Chao Sheng Chiang,
and Carl R. Daudt

Technical Report No. ONR-1-83

Project Period 10/1/81 to 3/30/83

Report Date 5/20/83

A

SECURITY CLASSIFICATION OF THIS PAGE (When Data Entered)

| REPORT DOCUMENTATION PAGE | | READ INSTRUCTIONS BEFORE COMPLETING FORM |
|---|---|---|
| 1. REPORT NUMBER<br>ONR-1-83 | 2. GOVT ACCESSION NO.<br>AD-A130 765 | 3. RECIPIENT'S CATALOG NUMBER |
| 4. TITLE (and Subtitle)<br>SYNTHETIC SEISMOGRAM CALCULATIONS FOR TWO-DIMENSIONAL VELOCITY MODELS | | 5. TYPE OF REPORT & PERIOD COVERED<br>Final Technical<br>10/1/81 to 3/30/83 |
| | | 6. PERFORMING ORG. REPORT NUMBER<br>ONR-1-83 |
| 7. AUTHOR(s)<br>Lawrence W. Braile, Chao Sheng Chiang, and Carl R. Daudt | | 8. CONTRACT OR GRANT NUMBER(s)<br>N00014-82-K-0033 |
| 9. PERFORMING ORGANIZATION NAME AND ADDRESS<br>Department of Geosciences<br>Purdue University<br>West Lafayette, IN 47907 | | 10. PROGRAM ELEMENT, PROJECT, TASK AREA & WORK UNIT NUMBERS |
| 11. CONTROLLING OFFICE NAME AND ADDRESS<br>ONR Resident Representative<br>Ohio State University Research Center<br>1314 Kinnear Road, Columbus, OH 43212 | | 12. REPORT DATE<br>5/20/83<br>13. NUMBER OF PAGES |
| 14. MONITORING AGENCY NAME & ADDRESS(if different from Controlling Office) | | 15. SECURITY CLASS. (of this report)<br>Unclassified<br>15a. DECLASSIFICATION/DOWNGRADING SCHEDULE<br>N/A |

16. DISTRIBUTION STATEMENT (of this Report)

Unlimited

17. DISTRIBUTION STATEMENT (of the abstract entered in Block 20, if different from Report)

Approved for public release: distribution unlimited

18. SUPPLEMENTARY NOTES

Synthetic Seismograms, Seismic Modeling, Finite Difference, Ray Theory

19. KEY WORDS (Continue on reverse side if necessary and identify by block number)

20. ABSTRACT (Continue on reverse side if necessary and identify by block number)

A variety of synthetic seismogram methods for laterally heterogeneous earth models have been developed and tested. Explicit finite difference methods for elastic wave propagation generally display high accuracy, but are limited in their application due to extensive computer time and storage requirements. Implicit finite difference methods may be able to realize a factor of eight improvement in computer time and a factor of four improvement in computer storage requirements as compared to explicit methods. The

DD FORM 1 JAN 73 1473 EDITION OF 1 NOV 65 IS OBSOLETE
S/N 0102-LF-014-6601

SECURITY CLASSIFICATION OF THIS PAGE (When Data Entered)

20.

Implicit methods of synthetic seismogram calculation are less well developed and are more difficult in the application of absorbing boundary conditions. Approximate methods using the scalar wave equation may also be useful for preliminary modeling of seismic data. A ray-theoretical method using ray tracing and disk ray theory (DRT) synthetic seismogram synthesis has been developed and compared to calculations using reflectivity (for 1-D) and finite difference (for 2-D) methods. The DRT method is fast and reasonably accurate making it very useful for routine modeling of 2-D seismic data. Its principal problem is the difficulty in tracing rays in certain complex geologic models. Various calculations of synthetic seismograms in laterally heterogeneous models and comparison with homogeneous models indicate the importance of including lateral heterogeneity, elastic wave propagation, proper source design and absorption in seismic modeling.

## ABSTRACT

A variety of synthetic seismogram methods for laterally heterogeneous earth models have been developed and tested. Explicit finite difference methods for elastic wave propagation generally display high accuracy, but are limited in their application due to extensive computer time and storage requirements. Implicit finite difference methods may be able to realize a factor of eight improvement in computer time and a factor of four improvement in computer storage requirements as compared to explicit methods. The implicit methods of synthetic seismogram calculation are less well developed and are more difficult in the application of absorbing boundary conditions. Approximate methods using the scalar wave equation may also be useful for preliminary modeling of seismic data. A ray-theoretical method using ray tracing and disk ray theory (DRT) synthetic seismogram synthesis has been developed and compared to calculations using reflectivity (for 1-D) and finite difference (for 2-D) methods. The DRT method is fast and reasonably accurate making it very useful for routine modeling of 2-D seismic data. Its principal problem is the difficulty in tracing rays in certain complex geologic models. Various calculations of synthetic seismograms in laterally heterogeneous models and comparison with homogeneous models indicates the importance of including lateral heterogeneity, elastic wave propagation, proper source design and absorption in seismic modeling.

# INTRODUCTION

We have been reviewing a variety of synthetic seismogram techniques for calculation in laterally inhomogeneous models for a number of years. In this report, we review progress on a variety of techniques including disk ray theory (DRT) based on ray theoretical methods and finite difference (FD) calculations which are based on direct numerical solutions to the seismic wave equation in two-dimensional laterally heterogeneous media. Both implicit and explicit formulas for finite difference calculations have been studied and we have utilized both the acoustic (scalar) and elastic wave equations for our finite difference methods. A review of our previous work in the field of synthetic seismogram modeling studies is included in Department of Geosciences, Purdue University, Report No. ONR-1-82 which was produced under contract with the Office of Naval Research, Contract No. N00014-75-C-0972. In this previous report, we described synthetic seismogram modeling studies including one-dimensional and preliminary work with two-dimensional models. In this report, we show a variety of synthetic seismogram calculations primarily for laterally heterogeneous models which illustrate the importance of lateral inhomogeneities in seismic wave propagation and compare a variety of approaches to synthetic seismogram calculations. Because these calculations can be extremely time consuming and require elaborate computer programs and extensive computer time and storage, we have spent considerable time on attempting to find more rapid methods which may be approximate, but would provide for preliminary modeling in two dimensions such that routine interpretation could utilize the vast and approximate techniques with final confirmation and checking relying on the more expensive and more accurate methods. Most of our examples are for wave propagation and earth models

corresponding to crustal seismology studies. However, the techniques that we describe are basically scale independent and can be used for studies of seismic wave propagation in models corresponding to shallow engineering studies (with depth of penetration of several tens of meters), to crustal studies (with depth of penetration of several tens of kilometers), and to whole earth models with propagation through the entire earth. Thus far our calculation techniques are limited to two-dimensional propagation and flat earth models, although it is conceivable that three-dimensional methods and spherical earth geometry could be utilized in the future.

## EFFECTS OF ACOUSTIC VERSUS ELASTIC WAVE PROPAGATION AND ANELASTICITY ($Q^{-1}$)

One approach to approximate calculation of synthetic seismograms in laterally inhomogeneous media is to utilize an acoustic wave equation approach as a preliminary modeling technique. An acoustic finite difference formulation for example is considerably faster than the equivalent elastic problem because of the relative simplicity of the scalar wave equation as compared to the complete elastic wave equation in two dimensions. In utilizing the scalar wave equation, the complete nature of seismic waves including the presence of shear waves and the possibility of P-S converted phases is not included. In addition, some of our finite difference methods utilize a perfectly elastic (infinite Q) calculation in contrast to the more realistic seismic wave propagation in which variable Q is included. For these reasons, we have calculated synthetic seismograms for a one-dimensional model for which the modified reflectivity method can be used to illustrate the effects of acoustic wave progagation and the effects of

including Q in the model by comparison with a calculation in which high Q and elastic propagation in included. Figure 1 illustrates a seismic record section calculated for an oceanic crustal model in which elastic wave propagation and high Q values are present. The model is shown to the left of the record section. The upper layer is a 200 m thick water layer in which the shear velocity is set to zero in the program and a density of 1.0 and a P wave velocity of 1.5 km/s is assumed. The source is within the water layer at a depth of 100 m. The source is approximately 10 Hz. Relatively high Q values are assumed in the sedimentary layer where a strong velocity gradient exists to a depth of about 4 km and in the oceanic crust and upper mantle beneath. The seismograms which result from this elastic and high Q calculation using the modified reflectivity method show a complicated wave propagation with a variety of P, multiple P, and P-S converted phases with a range of apparent velocity from the upper mantle (8 km/s) arrivals to a very low apparent velocity and low frequency arrival near the end of the seismograms. The high amplitude/high frequency arrival prominent on all of the seismograms is a water wave arrival with an apparent velocity of approximately 1.5 km/s. The low frequency arrival which arrives at slightly later times than the water wave is interpreted to be a shear wave or surface wave propagating in the sedimentary layer and coupled to water as an acoustic wave resulting in the low apparent velocity, low frequency, and obvious dispersion. In order to compare the effects of elasticity versus acoustic wave propagation, the identical model as shown in Figure 1 was utilized to calculate synthetic seismograms assuming purely acoustic wave propagation. The record section and the model are illustrated in Figure 2. Acoustic wave propagation in the modified reflectivity method is provided for by the transformation

suggested by Kind (1976). The acoustic seismograms shown in Figure 2 are very different from the synthetics for the elastic model. A water wave arrival is again present and is in fact stronger than the arrivals shown for the elastic model. However, most of earlier and higher apparent velocity phases are either much smaller or absent. In addition, the low apparent velocity/low frequency arrival is also absent. Finally, increased numerical noise due to trapping of a large percentage of the energy in the low velocity portions of the model resulting in large travel time arrivals and consequent time domain aliasing in the modified reflectiy method increases the numerical noise shown on the record section. The effects of Q are illustrated in Figure 3 in which the same elastic seismic model as shown in Figure 1 was used to calculate synthetic seismograms. However, the model shown in Figure 3 includes low Q values in the sedimentary layer and uppermost oceanic crustal layer. For this record section, all of the same arrivals that were included in the record section shown in Figure 1 are present, including the earlier high apparent arrivals, the water wave, and the low frequency/ low apparent velocity arrival. However, all of these phases are significantly attenuated and their amplitudes decrease fairly rapidly with distance due to the low Q values in the upper layers.

These examples serve to illustrate the importance of elastic wave propagation and the effects of Q in synthetic seismogram modeling. The elastic versus acoustic assumption appears to be particularly important. However, perfectly elastic and acoustic models may be useful for preliminary modeling as long as primary phases are of principle importance. Final interpretation of seismic data for real earth structures should include elastic wave propagation phenomena and the presence of Q structure.

# EXPLICIT FINITE DIFFERENCE METHODS

Explicit finite difference methods involve a direct numerical solution of the elastic wave equation in two dimensions for laterally heterogeneous media. In the explicit method, finite differences are used to approximate spatial and temporal derivatives in the elastic wave equation. Accuracy of the finite difference derivatives require that approximately 10 points per minimum wavelength of the waves propagated in the two-dimensional model be utilized. Because the displacements for time step T + 1 are calculated from two previous time steps (T and T-1), the time step must be chosen to be very small in order to maintain stability of the solution in this explicit method. Finite difference methods have been presented by Boore (1972), Alterman and Karal (1968) and Kelly et al. (1976). The calculations that we illustrate here are from the program developed by Mazzella (1979).

A flow chart illustrating the explicit finite difference synthetic seismogram calculation for acoustic or elastic wave propagation is shown in Figure 4. An arbitrarily complicated two-dimensional velocity model is described by a grid of seismic velocities. Source location, wavelet shape and peak frequency are designed which provide initial displacements for the iterative finite difference calculation. Displacements must be calculated for each grid point location for each time step of the model resulting in large grid point and time step loops in the computer program. Figure 5 illunstrates the calculation of a displacement at a particular grid location utilizing the nine grid points surrounding this location at times T and T-1. The spatial derivatives are obtained from the displacements at the nine grid locations at time equal T. The time derivative is obtained from the displacements at the grid location for times T and T-1. This process must be repeated for

all grid locations in the model. The finite difference model is illustrated in Figure 6. The two-dimensional velocity structure can be arbitrarly complicated with velocities given at each grid point. Absorbing boundary conditions (Clayton and Enquist, 1977, 1980 and Enquist and Majda, 1977) help to attenuate the fictitious reflections obtained from artifical boundaries of the model. A free surface boundary condition (Ilan, 1975) is included to account for the free surface conversion. The two-dimensional equations of motion for displacement in heterogeneous isotropic media and finite difference approximations for the explicit case for spatial derivatives and time derivatives are illustrated in Figure 7. The finite difference approximations are straight forward, but are reasonably complicated and lead to a long series of steps in a computer program. Some of the practical difficulties in applying explicit finite difference synthetic seismogram calculations are illustrated in Figure 8. Problems include approximations such as two-dimensionality and requirements of the grid spacing and time step which are related to the maximum frequency of waves which are to be propagated in the model. These requirements generally lead to large computer time and storage needs for calculation of realistic models.

In order to test our finite difference program, we have calculated synthetic seismograms using the modified reflectivity method and the finite difference program for a layer over a half-space model. The resulting record section (Figure 9) for vertical component seismograms show good comparison for primary P wave arrivals, multiples, and P-S conversions. Some discrepancy in surface wave arrivals is apparent due to the phase velocity range included in the modified reflectivity method calculation and due to the presence of some numerical dispersion

in the finite difference calculation for the relatively short wavelength surface waves due to their low propagation velocity. A more detailed comparison of the seismograms for the finite difference and modified reflectivity methods is shown in Figure 10 for distances of 10, 20, 30 and 40 km. The modified reflectivity seismograms for these distances are illustrated immediately beneath the finite difference seismograms. Good amplitude and waveform comparison is seen for all phases except the surface wave.

The finite difference elastic wave equation method represents an accurate numerical technique for the calculation of two-dimensional synthetic seismograms in laterally heterogeneous media. At present, computer limitations preclude its use in routine modeling of seismic data. For most models of geophysical and geological interest, the finite difference calculation of realistic synthetics with the finite difference program would require computer time on the order of several hours using the fastest computers available (Cray 1 and Cyber 205) and in addition would require core storage of greater than a million words. Therefore, we consider the finite difference approach at the present time to be primarily of interest for model studies in which various kinds of wave propagation phenomena can be studied with seismograms for characteristic models. In addition, the finite difference program synthetics represent an important check on faster, but more approximate techniques.

## DISK RAY THEORY SYNTHETIC SEISMOGRAM METHOD

A disk ray theory (DRT) synthetic seismogram method for approximate calculation of seismic wave propagation in laterally heterogeneous elastic

and anelastic media has been developed and tested. The disk ray theory method follows the theory developed by Wiggins and Madrid (1974) and Wiggins (1976). The technique utilizes ray tracing and complex two-dimensional velocity and Q models to provide the necessary time distance and amplitude data to construct synthetic seismograms by a summation of the contribuitons of the various raypaths. A description of the technique and some examples of its application are shown in a paper entitled "An Example of Application of Synthetic Seismogram Modeling in Two Dimensions" by C.S. Chiang and L.W. Braile. A copy of this paper is included in the Appendix to this report.

The principal advantage of the DRT synthetic seismogram method is speed. It is relatively accurate and synthetics can be quickly constructed for two-(or even three-) dimensional models for which ray tracing can be performed. The method can include primary P and S phases as well as multiples (Figure 11). Its principal limitation is that guided or interference propagation type of phases cannot be included. Surface waves are not accounted for and some geologic models are difficult or impossible to trace rays through so that the necessary ray trace input may not be available for certain physically important phases. An example of a DRT calculation is illustrated for the model shown in Figure 12. The seismic raypaths are traced using a ray tracing program for the phases shown. Amplitude, travel time, raypath parameter and distance date are then used to construct synthetic seismograms by the DRT method. For this relatively simple, but important laterally inhomogeneous fault model, the seismic rays can be traced with high accuracy and efficiency to produce the data for the DRT seismogram synthesis. This model, however, illustrates one of the problems with the DRT method. The seismic phases shown in Figure 12 corresponding

to the propagation at the bottom of the prominent fault (Phases $P_{refl-2}$ and $P_{h-2}$) cannot be traced directly in this model. If one attempts to trace these raypaths from the source to the bottom of the fault plane (corner) the raypaths do not refract by Snell's Law to the received locations as shown. In fact, the lower corner of the fault represents a diffractor. However, we know from wave theoretical principals and from a finite difference calculation that the waves corresponding to these raypaths are physically important and are present in the seismic wave propagation in this model. Therefore, we were able to generate these phases by a two step ray tracing procedure. All other phases were ray traced in the normal method from source to reflecting or refracting point and then to receiver. However, for these two phases, rays were traced from the source to the diffraction point (corner at the bottom of the fault). Then, an artifical source was located at this corner and caused to generate the phases $P_{refl-2}$ and $P_{h-2}$. The travel time and amplitude factors for this artifical diffraction source were then combined with the raypaths from the source to the corner to obtain the time distance and amplitude factors necessary for DRT synthesis for these complicated raypaths. In this way, the correct wave propagation phenomena were simulated. However, the amplitude factors which resulted from this calculation were too large of amplitude for these two phases from the point diffractor. By assuming that the effective reflection coefficient of the point diffractor at the corner of the fault was approximately 0.3, seismograms from the DRT method which compare favorably with finite difference synthetic were produced (Figure 13). The finite difference and DRT synthetics for the fault model (INFL-11) shows excellent comparison for all of the primary arrivals. Later arrivals (multiple P waves, P-S conversions

and surface waves) included in the finite difference calculation are not included in the DRT synthesis. In addition, the wide angle reflection from the upper interface (Phase $P_{refl-1}$) has too large of an amplitude at large distances for the DRT method. This is a result of the limitation of ray theory for grazing incidence wave propagation at low frequencies for thin layers. However, this is not severe limitation of the DRT method because such arrivals are rarely of significance anyway because of the lower apparent velocity of such phases and the presence of attenuation which normally decreases their amplitudes fairly rapidly. A more detailed comparison of the finite difference and disk ray theory synthetics for the fault model (INFL-11) is shown in Figure 14. Amplitude and wave form character of phases of interest are nearly identical for the FD and DRT method. Therefore, we conclude that the DRT method provides a very useful approach to preliminary modeling of seismic data in two-dimensional or even three-dimensional media. The technique is fast, reasonably accurate and is limited only due to the difficulty of tracing rays for certain phases and certain geological models. We suggest that this technique would provide a very useful modeling method in which routine ray-tracing and DRT synthesis can provide comparison with observed seismic data for two-dimensional velocity structures. For final confirmation or where the technique is not appropriate, finite difference or other wave theortical techniques will still be necessary.

## FINITE DIFFERENCE SYNTHETIC SEISMOGRAM CALCULATIONS FOR DISLOCATION SOURCE MODELS.

Explicit finite difference synthetic seismogram calculations program for dislocations source models has been presented by Espindola

(1979). The technique follows similar methods as illustrated previously in this report and are also similar to those presented by Mazzella (1979). However, in this method a skew symmetric coordinate system (Figure 15) is utilized to provide for a distributed dislocation source which simulates an earthquake. A dislocation with arbitrary slip function and source time history is caused to occur at grid points corresponding to the source fault plane location. Finite difference calculations allow for propagation of seismic waves away from this distributed source. The skew symmetric coordinate system is required in order to provide for parallellism of the grid spacing with the source fault plane. This program therefore, has an additional advantage over the previously described finite difference program in that a variety of more realistic source phenomena can be studies using the finite difference method. The program of the method still utilizes the explicit approach and is limited, therefore requiring certain grid point and time step conditions, necessitating large computer time and storage and is also limited to a two-dimensional approximation such that the source fault plane is assumed to extend in the direction perpendicular to the XZ axis. Examples of synthetic seismogram calculations using this dislocation finite difference method are shown for a homogeneous half space model (Figure 16) and a complicated laterally heterogeneous velocity structure model (Figure 17). A variety of source slip functions and source time histories for the identical fault geometry (Figure 18) are also illustrated. Figure 19 shows the seismic ray paths which are produced by the distributed source dislocation for a simple displacement time history. The prominent effects of two-dimensionality can be illustrated by comparing seismograms calculated for the homogeneous and the laterally heterogeneous models. Figure 20

shows vertical and radial component seismograms (WWSSN response) calculated for model S-2 with a ramp function displacement time history. Comparison of selected seismograms for the homogeneous and laterally heterogeneous calculations (models S-1A and S-2A) are shown in Figure 21. Both short period and long period WWSSN seismograms responses are shown. The effects of inhomogeneity are prominent primarily in later arriving phases on Z and R components of model S-2A and in the large amplitude phase which is present primarily on the radial component for model S-2A. Long period records also show considerable difference in wave form due to the wave propagation and the complex structure. The identical source is used for both of these models.

Comparison of the effects of differing source functions is illustrated in the seismograms shown in Figure 22. All of these synthetic seismograms are calculated for the identical homogeneous half space model and identical fault geometry (Figure 16 and Figure 18). However, the source time history and slip functions illustrated in Figure 18 were used for calculations S-1A, S-1B and S-1C. The ramp source time history (S-1A) produces considerably more high frequency wave propagation and more complex phase arrivals than for the smoother slip function and time history calculations.

These calculations serve to illustrate the utility of the finite difference method for application to earthquake problems in which the source function is of significance and also to demonstrate the importance of lateral heterogeneity in wave propagation for models of complex geologic structure.

## IMPLICIT FINITE DIFFERENCE SYNTHETIC SEISMOGRAMS CALCULATIONS

We have pursued the use of implicit numerical techniques in finite difference formulations, in hopes of reducing both computer time and storage requirements of existing predominately explicit formulations. Implicit techniques, which involve centered-differences calculations at each time step, have two potential advantages over explicit formulations. Firstly, some of the implicit formulations are numerically stable for any step size and grid spacing. This characteristic allows the length of the time steps to be increased, thus decreasing the actual number of time steps without any regard for stability. One must use caution in increasing the size of the time step, however, to insure that the accuracy is maintained. Secondly, another potential advantage of implicit formulations is that some of the techniques are more accurate than their explicit couterparts. Thus, a coarser grid spacing along with a corresponding increase in time step size is afforded while maintaining accuracy and stability for certain implicit formulations with higher accuracy. In general, our experimentation indicates a trade off between stability and accuracy of implicit formulations. If both time steps and grid spacings can be increased, significant savings in computer time and storage requirements may be possible with implicit methods. For the most part our implicit studies have utilized the simpler scalar (acoustic) wave equations. Experience with these techniques indicates that further application to the elastic wave equation may be warranted. However, additional problems, such as the difficulty of applying absorbing boundary conditions to the more complicated implicit formulas for the elastic case may diminish some of the anticipated benefits of implicit formulas.

The principle disadvantage of implicit finite difference formulations are primarily concerned with their complexity. Implicit calculations are not as straight forward as their explicit couterparts (Figure 23 and Figure 24). Implicit difference equations for two or three-dimensional problems have to be broken down corresponding to two or three elements using either an alternating direction implicit (ADI) or a locally one dimensional (LOD) spliting technique. Each of these parts must be solved inversely using a tri-diagonal matrix equation solver. These equations are particularly difficult to formulate for a fully absorbing boundary condition at the edges and bottom of the model, and for a free surface boundary condition at the top of the model.

We have compared both with accuracy calculations and actual implicit finite difference programs, a variety of implicit finite difference techniques (Figure 25). The different formulas illustrated in Figure 25 have different accuracy and stability conditions and the complexity of the formulas leads to differing degrees of difficulty in applying boundary conditions source functions and other practical aspects of producing a workable finite difference program for two-dimensional seismic wave propagation problems.

One of our most significant experimental results has come from comparing four different implicit formulations of the scalar wave equation with an explicit formulation for accuracy. Our accuracy criterian is derived from the numerical dispersion studies published by Alford et al. (1974) and Emerman et al. (1982). However, we have investigated the numerical dispersion effects of all the formulas shown in Figure 25. Some of the results are illustrated in Figures 26 through 29. While some of implicit formulations prove to be less accurate than the explicit case, the equations proposed by Fairweather and Mitchell

prove to be far superior. For example, one can see from the explicit accuracy diagram shown in Figure 26 that in order to maintain reasonable accuracy in an explicit solution, one must use approximately ten points per wave length ($\frac{l}{G}$ = 0.1) in order to prevent significant numerical dispersion. This ten points per wave length requirement, in addition to the small times step required for stability, makes the explicit case extremely costly in computer time and storage. The implicit finite difference formula presented by Emerman, Schmidt and Stephen (1982) does not have the stability requirement, however, one can see from Figure 27 that a small time step is again required in order to maintain reasonable accuracy. Further, the accuracy of the solution decreases with increasing time step (increasing p value) making this formulation rather undesirable because although the time step can be increased and stability still maintained thus improving on computer time, the grid spacing must be kept extremely small (greater than 10 points per wave length) in order to maintain accuracy. However, the numerical dispersion accuracy curves (Figure 28 and Figure 29) for the Fairweather and Mitchell (1965) formula show that this formula is far superior. For this case, minimal dispersion is observed for as few as four to five grid points per wave length ($\frac{l}{G}$ = 0.2 to 0.25) and for a variety of time step conditions (p = 0.1 to p = 0.7), thus one can maintain reasonable accuracy with the Fairweather and Mitchell formula with approximately twice as coarse of a grid spacing as for the explicit or other implicit methods. For a two-dimensional model these conditions result in a factor of four savings in computer storage and of eight savings in computer time, because the time step can also be increased as the grid spacing is increased. The Fairweather and Mitchell formula, however, does have a stability limit, such that the time step can only

be increased to p = 0.7. Nevertheless, this potential savings in computer time of approximately a factor of eight and a savings of computer storage requirements of approximately a factor of four make the Fairweather and Mitchell implicit formula worth investigating further.

We have developed working programs using the implicit finite difference formulation for the acoustic (scalar) wave equation. We have used both the Emerman, Schmidt and Stephen implicit formulas as well as the Fairweather and Mitchell formulas. Although further analysis is required and detailed comparisons of accuracy, stability and calculation time between the two implicit methods and the explicit approach are required, we believe that the Fairweather and Mitchell implicit finite difference method will be useful for further application to synthetic seismogram calculation in two-dimensional models. We have succeeded in applying relatively accurate non-absorbing boundary conditions, at the edges of implicit models (Figure 30). However, the higher order absorbing boundary conditions need to be applied to the Fairweather and Mitchell formulas and these implicit techniques need to be applied to the elastic wave equation case in order to fully realize the benefits of implicit difference methods in two-dimensional synthetic siesmogram calculation.

# REFERENCES

Alford, R.M., K.R. Kelly, and D.M. Boore, Accuracy of finite-difference modeling of the acoustic wave equation, Geophysics, 39, p. 834-842, 1974.

Alterman, Z., and F.C. Karal, Jr., Propagation of elastic waves in layered media by finite difference methods, Bull. Seismological Soc. America, 58, p. 367-398, 1968.

Boore, D., Finite difference methods for seismic wave propagation in heterogeneous materials in Methods in Computational Physics, v. 11, B. Bolt, Ed., New York, Academic Press Inc., 1972.

Clayton, R., and B. Enquist, Absorbing boundary conditions for acoustic and elastic wave equations, Bull. Seismological Soc. America, 67, p. 1529-1540, 1977.

Clayton, R., and B. Enquist, Absorbing boundary conditions for wave-equation migration, Geophysics, 45, p. 895-904, 1980.

Emerman, S.H., Schmidt, W. and R.A. Stephen, An implicit finite-difference formulation of the elastic wave equation. Geophysics, v. 47, No. 11, p. 1521-1526, 1982.

Engquist, B., and A. Majda, Absorbing Boundary conditions for the Numerical Simulation of Waves, Mathematics of Computation, 31, p. 629-651, 1977.

Espindola, J.M., Finite difference synthetic seismograms for kinematic models of the earthquake source, Ph.D. thesis, Purdue University, West Lafayette, IN., p. 151, 1979.

Fairweather, G., and A.R. Mitchell, A high accuracy alternating direction method for the wave equation, J. Inst. Maths. Applics, 1, p. 309-316, 1965.

Ilan, A., Ungar, A., and Alterman, Z., An improved representation of boundary conditions in finite difference schemes for seismological problems: Geophys, J. Roy. Astron. Soc. London, v. 43, p. 727-745, 1975.

Kelly, K.R., R.W. Ward, S. Treitel, and R.M. Alford, Synthetic seismograms; a finite-difference approach, Geophysics 41, p. 2-27, 1976.

Kind, R., Computation of Reflection Coefficients for Layered Media, J. Geophys., 42, p. 191-200, 1976.

Lees, M., Alternating direction methods for hyperbolic differential equations, J. Soc. Indust. Appl. Math, 10, p. 610-616, 1962.

Mazzella, F.E., The generation of synthetic seismograms for laterally heterogeneous models using the finite difference tachnique, Ph.D. thesis, Purdue University, West Lafayette, In., p. 225, 1979.

Samarskii, A.A., Local one dimensional difference schemes for multi-dimensional hyperbolic equations in an arbitrary region, Z. Vycisl. Mat. Z. Mat. Fiz., 4, p. 21-35, 1964.

Wiggins, R.A. and M.A. Madrid, Body wave amplitude calculations, Geophys. J.R. Astr. Soc., 37, p. 423-433, 1974.

Wiggins, R.A., Body Wave Amplitude Calculations-II, Geophys. J.R. Astr. Soc., 46, p. 1-10, 1976.

# FIGURE CAPTIONS

Figure 1. Synthetic seismograms calculated for a plane layered shallow oceanic model. The calculation includes the effects of elastic wave propagation in the oceanic crustal layers beneath a 200 meter depth and acoustic wave propagation in the upper water layer (200 meters thick). The frequency of the source is approximately 10 Hz and the source depth is 100 meters. High Q values ($Q_p$ = 1,000, 500, 1,000 are assumed for the water layer, sedimentary layer and oceanic crustal and upper mantle layers, respectively). Amplitudes are scaled for plotting by multiplying the amplitude of each seismogram by the distance.

Figure 2. Synthetic seismograms calculated for an acoustic layered half-space. The layer parameters are the same as for Figure 1. Acoustic wave propagation is simulated in both the water layer and the oceanic crustal and upper mantle layers. High Q values, as in Figure 1, are assumed. The acoustic propagation in the reflectivity program is simulated by the transformation described by Kind, 1976. Some numerical noise in the calculation is evident throughout the record section. The amplitudes for this seismogram are scaled to one-half of the amplitudes shown on Figure 1.

Figure 3. Synthetic seismograms calculated for the identical oceanic model as in Figure 1, except that low Q values are included in the sedimentary layer and the upper oceanic crystal layer. An elastic half-space beneath the acoustic water layer (thickness of 200 meters) is assumed. Amplitude scaling is identical to that shown on Figure 1.

Figure 4. Flow chart for the calculation of finite difference synthetic seismograms for acoustic or elastic earth models using the explicit finite difference formulation.

Figure 5. Illunstration of the computational technique for spatial and temporal finite difference derivatives at a time T+1 using the surrounding displacement grid points at times T and T-1.

Figure 6. Schematic diagram illustrating the calculation of finite difference synthetic seismograms for a two-dimensional earth model. The velocity structure is approximated by a grid in which the seismic velocity is given at each grid location. Seismic waves are caused to propagate by a finite difference time step calculation away from an arbitrarily located source point. A free surface boundary condition and absorbing boundaries at the fictitious edges of the model are included. Seismometer locations record the displacement time history for the wave propagation in the two-dimensional model.

Figure 7. Two-dimensional equations of motion for displacement in heterogeneous isotropic media and finite difference approximations for the explicit finite difference formulation of second order spatial derivatives, cross-product spatial derivatives and second order time derivatives for approximations to the two-dimensional equation of motion.

Figure 8. List of some of the practical aspects of explicit finite difference synthetic seismogram calculation.

Figure 9. An example of finite difference synthetic seismogram calculation in a laterally homogeneous media. Upper record section shows synthetic seismograms calculated for a layer over a half-space model using the modified reflectivity method. Lower record Section shows synthetic seismograms calculated by the finite difference technique for the identical model. The model consisted of a 2 km thick 4.5 km/s layer overlying a 6 km/s half-space. In the upper diagram, amplitudes are scaled by distance squared. In the lower record section, amplitudes are scaled by distance to the one power. The difference in amplitude scaling corresponds to the difference in assumptions of the two methods. In the modified reflectivity method, a point source in a one-dimensional model represents three-dimensional spreading of the wave energy. In the finite difference model, however, a two-dimensional approximation is assumed and the source is actually a line source.

Some differences in the later portions of the record section are observable due to the fact that the surface waves were not exactly included in this particular calculation using the modified reflectivity method and also due to the fact that because of the choice of grid spacing and time step parameters in the finite difference calculation, some numerical dispersion is included for shear wave and surface wave propagation. However, the compressional waves for primary and multiple reflections are correctly included in both methods and a comparison of the two synthetic seismogram record sections indicates that the finite difference seismograms are nearly identical to the modified reflectivity method seismograms.

Figure 10. Comparison of finite difference and modified reflectivity synthetic seismograms for the layer over a half-space model described in Figure 9. These seismograms illustrate a detailed comparison of the synthetics at distances of 10, 20, 30 and 40 km from the source.

Figure 11. Synthetic seismograms calculated for the modified reflectivity and disk ray theory methods for a layer over a half-space model including primary compressional waves, first order multiples and selected P-S conversions. The DRT synthetics are shifted slightly to the left of their proper distance for convenient display and comparison with the MRM seismograms. Amplitudes of the seismograms are scaled by distance to the one power for convenient plotting.

Figure 12. Seismic raypaths for DRT calculation for fault model INFL-11.

Figure 13. Seismic record sections for finite difference and disk ray theory synthetic seismograms for fault model INFL-11. Seismic phases are identified for the raypaths shown in Figure 12. Finite difference synthetic seismograms are scaled by multiplying by distance to the one power, whereas the disk ray theory synthetics are scaled by multiplying by the distance squared to account for the difference in line source for the finite difference program versus point source for the disk ray theory program. Multiples and P-S converted phases are not included for the disk ray theory calculation, but are included in the finite difference model.

Figure 14. Comparison of finite difference and disk ray theory synthetics for fault model INFL-11 for distances 10, 20, 30, 40 and 50 km. Phase notation is identical to that shown on the raypath diagram (Figure 12).

Figure 15. Schematic diagram illustrating the grid geometry for finite difference model calculations in a skew coordinate system with a dislocation (earthquake) source.

Figure 16. Homogeneous half-space model for skew coordinate system finite difference calculation. The source is a reversed fault beneath seismometer location number 6. The source time history is shown as an inset in the model. A unilateral source is assumed with fracturing beginning at the lower end of the fault plane.

Figure 17. A laterally inhomogeneous earth model, representing a subduction zone, with identical geometry and source to the homogeneous model shown in Figure 16.

Figure 18. Diagram illustrating the fault geometry slip functions and source time histories for a variety of calculations using the skew symmetric coordinate system finite difference synthetic seismogram program.

Figure 19. Schematic diagram illustrating the seismic raypaths which produce prominent arrivals from a dipping fault source for a ramp function displacement in the homogeneous half-space model (Figure 16). Dashed raypaths indicate S wave propagation and solid raypaths indicate compressional wave propagation. Unprimed phase notation indicates arrivals from the starting phase of the source time history, whereas primed phases are due to the stopping phase two seconds after the initiation of fracturing. Subscript 1 indicates arrivals from the point of initiation of fracture at the bottom of the fault plane. Subscript 2 indicates arrivals propagating from the top end of the fault plane.

Figure 20. Synthetic seismograms calculated for model S2 (Figure 17) for vertical and radial component displacements. The seismograms have been convolved with a seismograph response function corresponding to a short period WWSSN response. Seismograms are plotted as a function of distance from the zero point directly above the point of initiation of the earthquake source. Small numbers adjacent to the seismograms indicate the seismometer position. Relative amplitudes are constant for all seismograms and can be compared with the relative amplitude scale shown at the bottom of the record section.

Figure 21. Comparison of short period and long period seismograms for models S1A and S2A at a distance of -6.1 km corresponding to seismometer number 6. Both vertical (SPZ and LPZ) and radial (SPR and LPR) seismograms are shown. The long period records are scaled with a difference amplitude scale as indicated at the bottom of the diagram.

Figure 22. Comparison of SPZ seismograms for the homogeneous half-space fault model (Figure 16) with the three difference source functions (1A, 1B, 1C) illustrated in Figure 18. The phase notation is the same as illustrated in Figure 19. Dotted lines indicate portions of seismograms with an enhanced amplitude scale to see small arrivals. The amplitude scales differ for each of the record sections and are scaled according to the relative amplitude scale bar shown at the bottom of each record section.

Figure 23. Equations used in calculating acoustic finite difference synthetic seismograms using the scalar wave equation. An explicit and an implicit finite difference form are illustrated as well as second order finite difference operators.

Figure 24. Schematic diagram illustrating the method of propagation of pressures at time N+1 from times N and N-1 using the explicit finite difference form as well as a similar diagram illustrating the same calculation using the implicit form.

Figure 25. Five different finite difference schemes for explicit and implicit finite difference calculations using the scalar (acoustic) wave equation.

Figure 26. Accuracy diagram for the explicit acoustic wave equation. The normalized phase velocity is a measure of the degree of numerical dispersion present in the calculation for a variety of grid spacings. The value of 1/G of 0.1 which corresponds to 10 points per wavelength is normally considered appropriate for explicit finite difference calculations to maintain a negligible amount of numerical dispersion. The calculation is for an angle of incidence with respect to the grid axes of 0°. The P values are relative to the time step of the calculation where $P = C_0 \times \Delta T/\Delta X$.

Figure 27. Accuracy diagram for the implicit formula given by Emerman, Schmidt and Stephen (1982).

Figure 28. Accuracy diagram for the implicit finite difference equation given by Fairweather and Mitchell (1965).

Figure 29. Accuracy diagram for the implicit finite difference formula given by Fairweather and Mitchell (1965). In this case, the P value is kept constant at 0.7 and the various angles of incidence from 0 to 45° are assumed.

Figure 30. Displacement time history diagrams (snapshots) of an implicit finite difference calculation in a homogeneous media in two dimensions. The two-dimensional space and the displacements are illustrated in a perspective view. The edges of the perspective diagram correspond to the artifical edges of the model. A non-reflecting boundary condition is assumed and relatively small amounts of energy are reflected back from the boundaries.

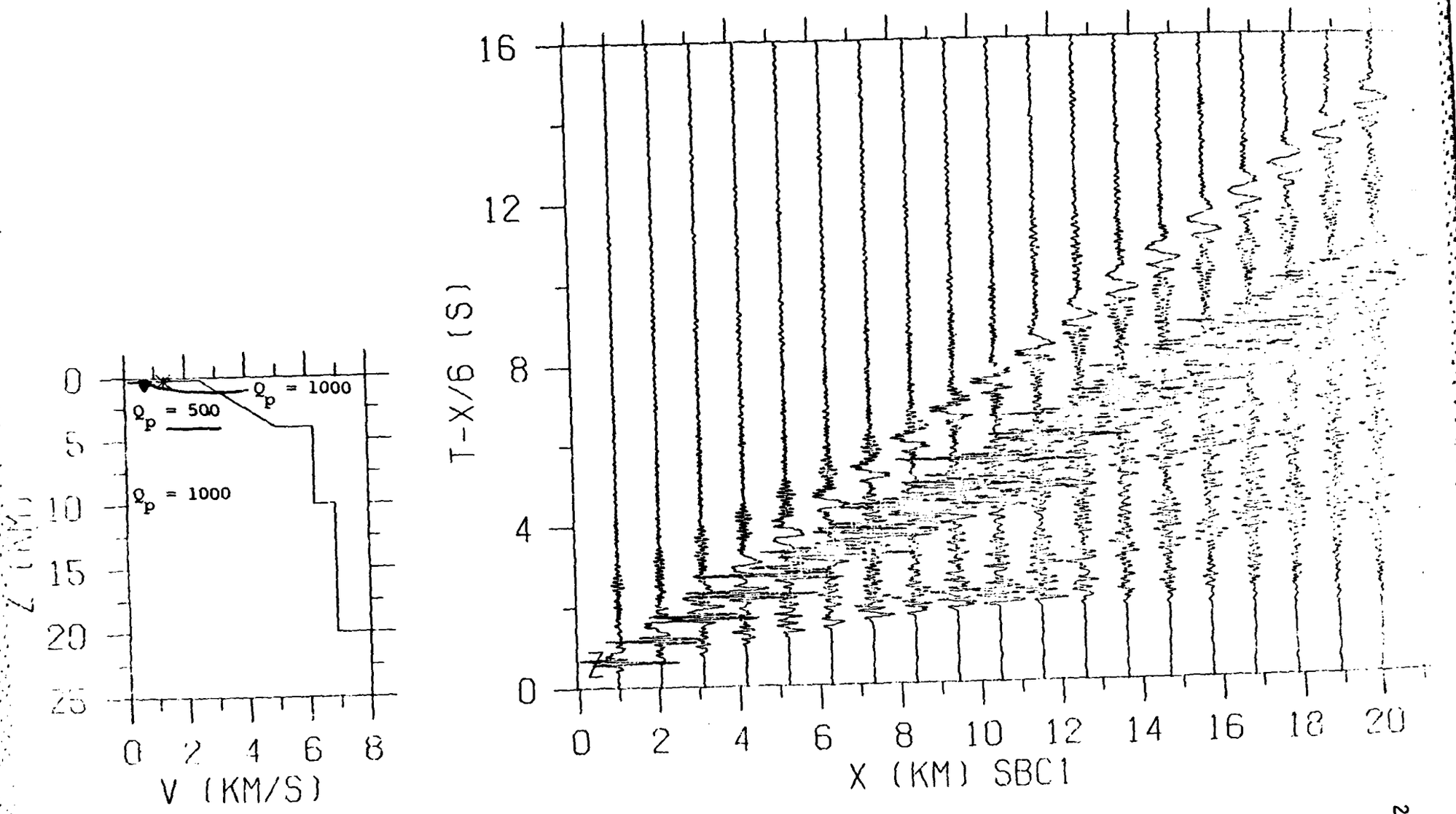
Z (KM)
0
5
10
15
20
25
$Q_p$ = 1000
$Q_p$ = 500
$Q_p$ = 1000
0 2 4 6 8
V (KM/S)
T-X/6 (S)
16
12
8
4
0
Z
0 2 4 6 8 10 12 14 16 18 20
X (KM) SBC1

Figure 1.

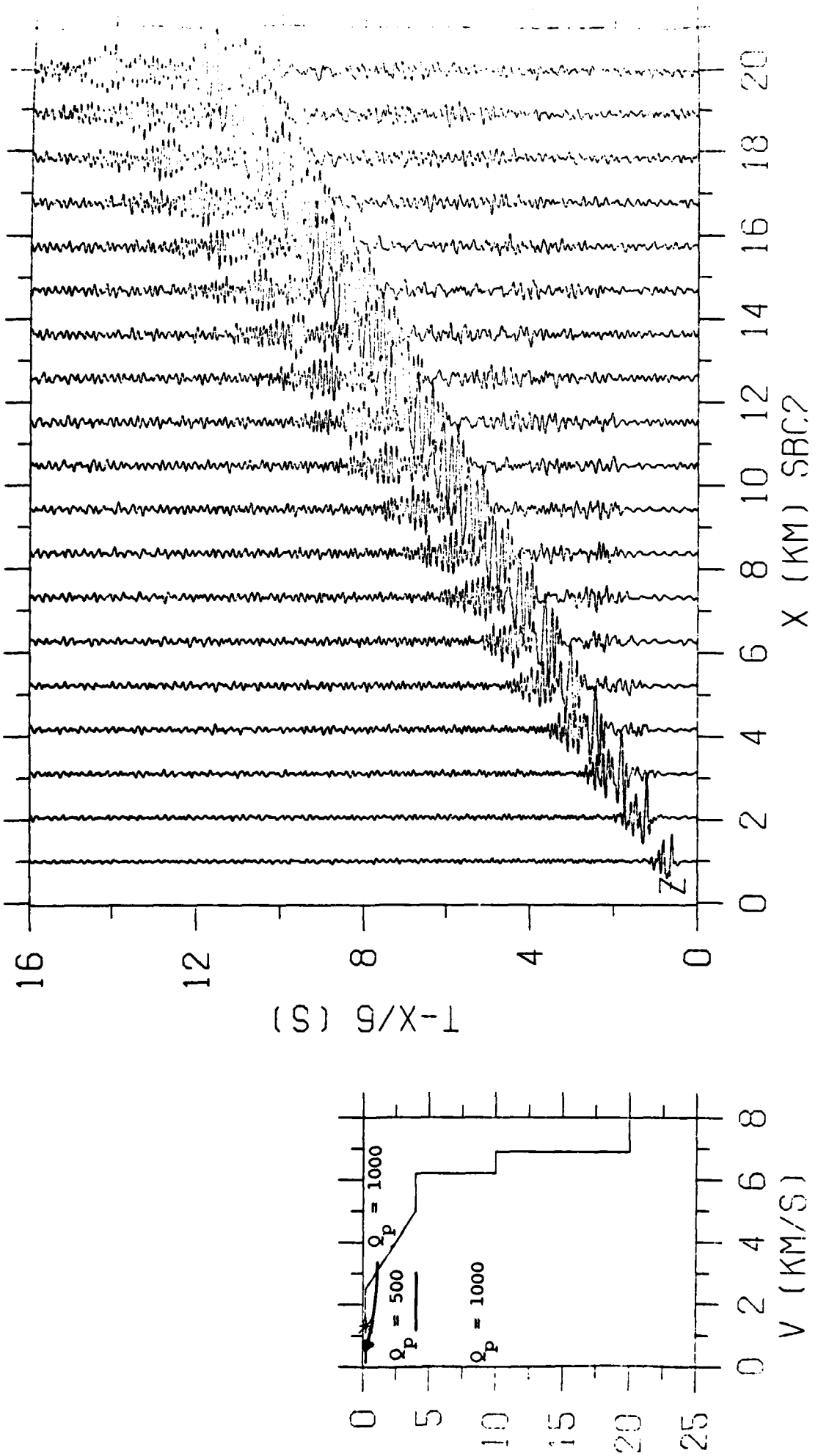
X (KM) SRCV
0 2 4 6 8 10 12 14 16 18 20
Z
T-X/6 (S)
16 12 8 4 0
V (KM/S)
0 2 4 6 8
$Q_p$ = 1000
$Q_p$ = 500
$Q_p$ = 1000
0 5 10 15 20 25

Figure 2.

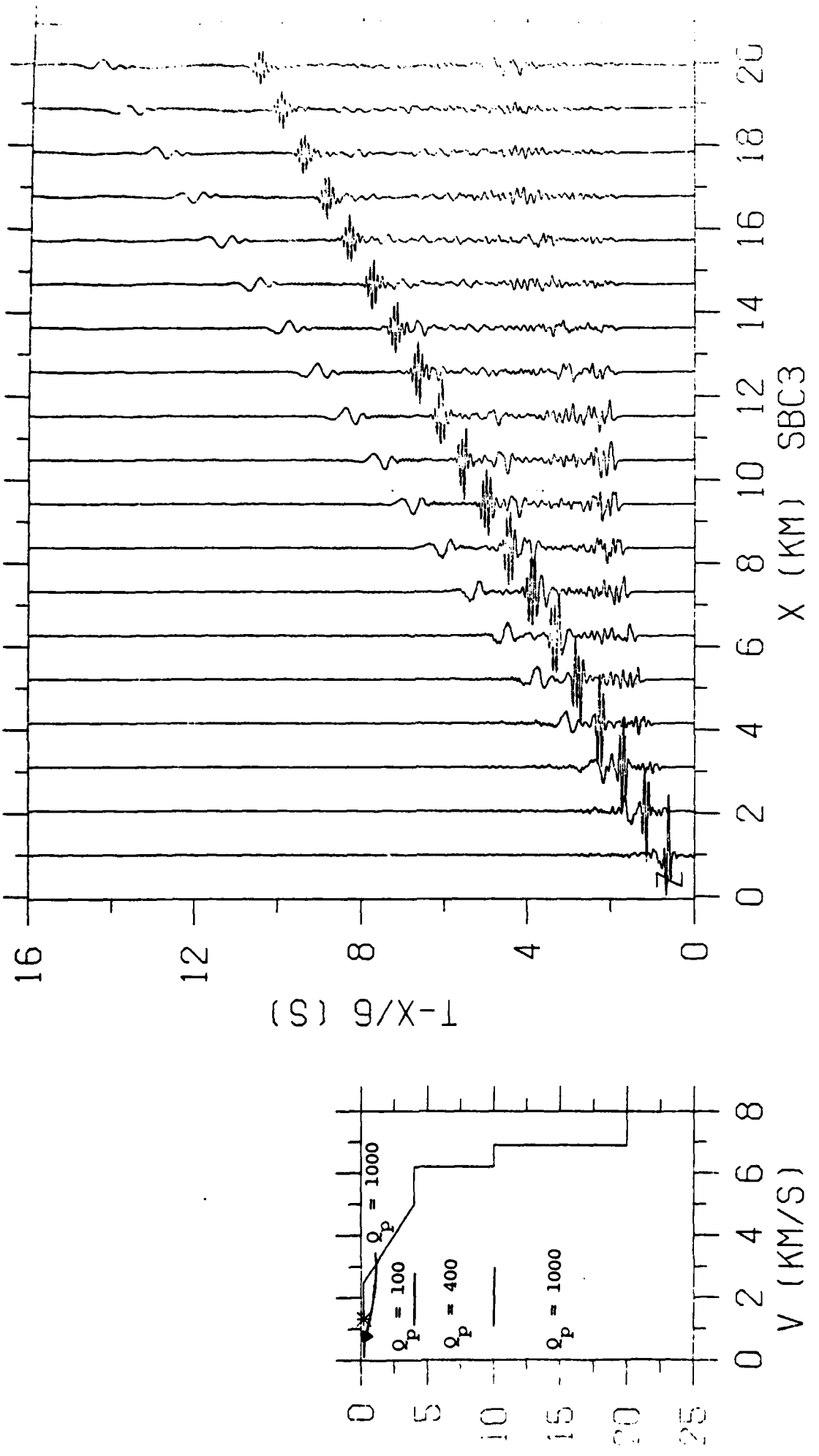
T-X/6 (S)
16
12
8
4
0
0 2 4 6 8 10 12 14 16 18 20
X (KM) SBC3
Z
V (KM/S)
0 2 4 6 8
0 5 10 15 20 25
$Q_p$ = 1000
$Q_p$ = 100
$Q_p$ = 400
$Q_p$ = 1000

Figure 3.

FLOW - CHART FOR FINITE DIFFERENCE SYNTHETIC SEISMOGRAM CALCULATION FOR ACOUSTIC ( $\alpha(x,z)$ ) OR ELASTIC ( $\alpha(x,z)$, $\beta(x,z)$, $\rho(x,z)$ ) CASE

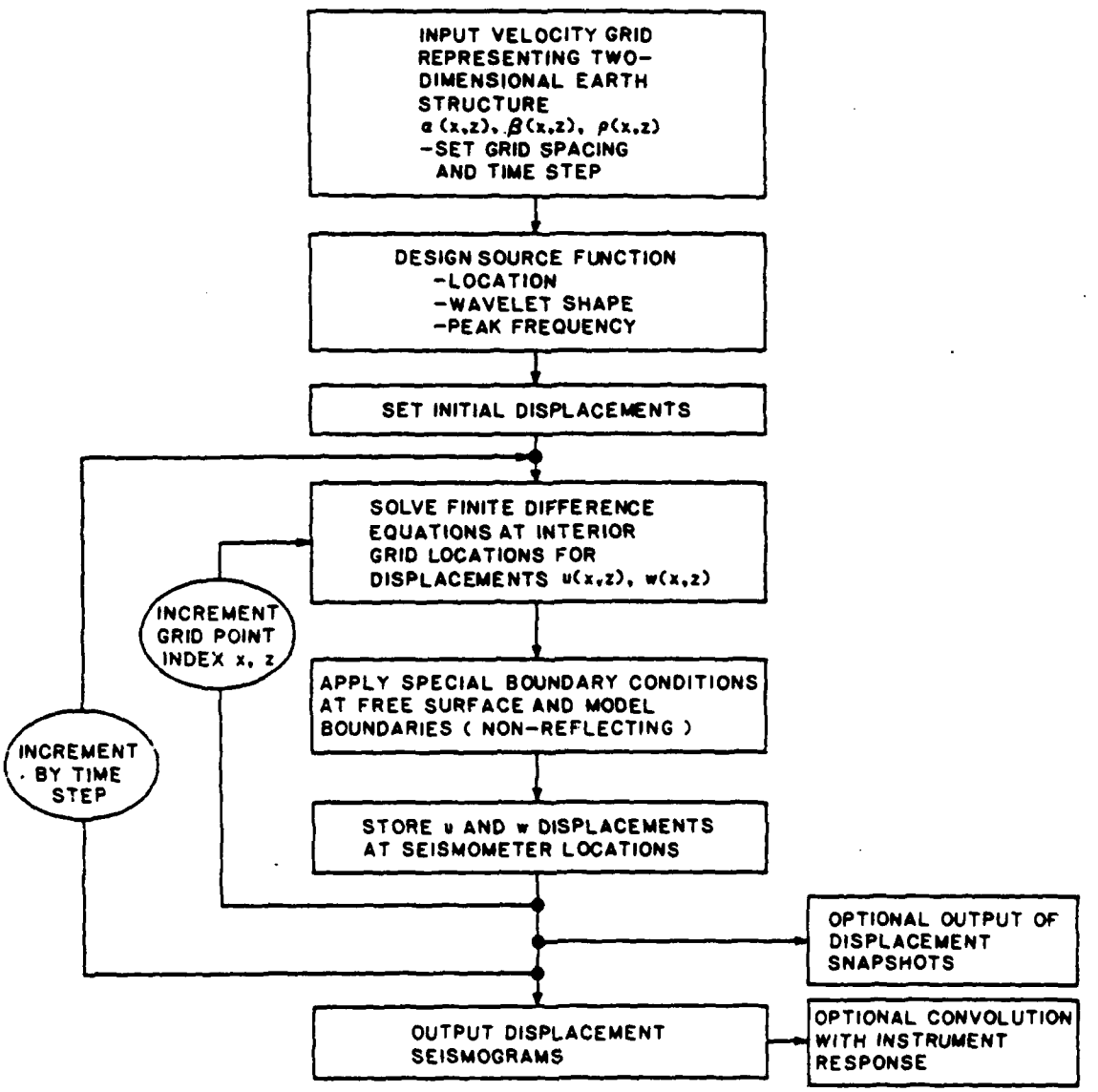


Figure 4.

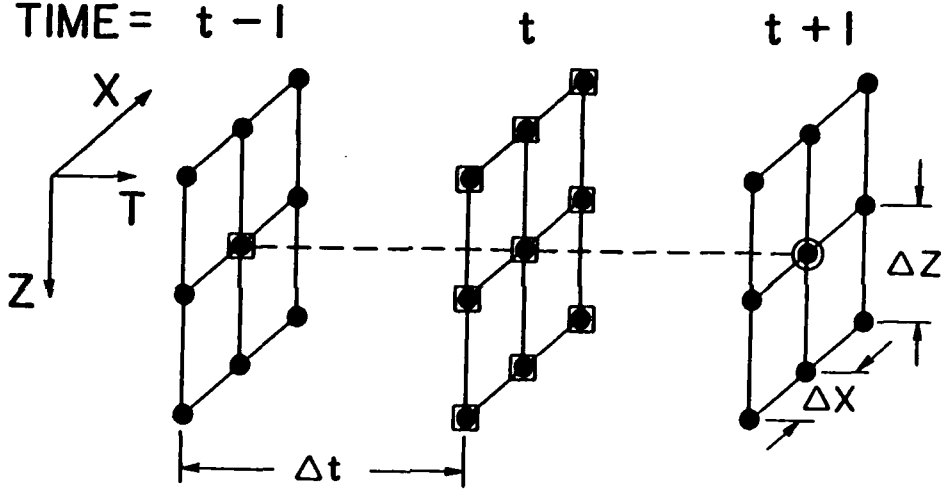


GRID POINTS REQUIRED (■) FOR COMPUTATION OF DISPLACEMENTS AT TIME t+1 USING SPATIAL AND TEMPORAL FINITE DIFFERENCE DERIVATIVES

Figure 5.

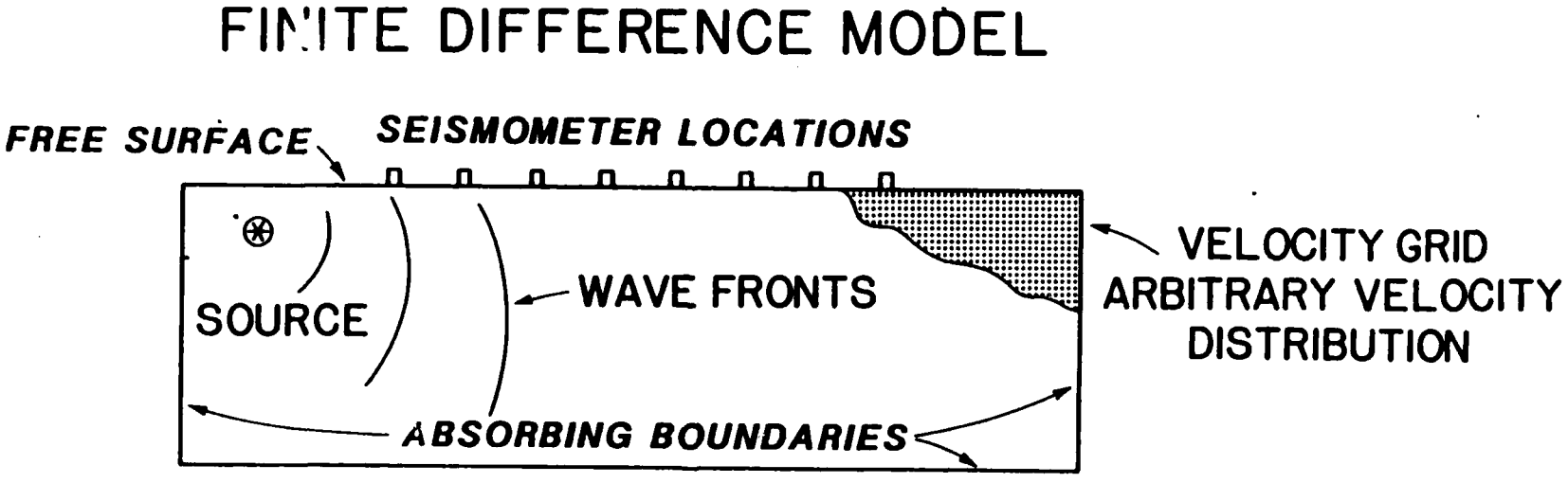
FINITE DIFFERENCE MODEL
FREE SURFACE
SEISMOMETER LOCATIONS
SOURCE
WAVE FRONTS
VELOCITY GRID
ARBITRARY VELOCITY
DISTRIBUTION
ABSORBING BOUNDARIES

Figure 6.

## TWO DIMENSIONAL EQUATIONS OF MOTION FOR DISPLACEMENT ( HETEROGENEOUS, ISOTROPIC MEDIA )

$$\rho \frac{\partial^2 u}{\partial t^2} = \frac{\partial}{\partial x}\left[\lambda\left(\frac{\partial u}{\partial x}+\frac{\partial w}{\partial z}\right)+2\mu\frac{\partial u}{\partial x}\right] + \frac{\partial}{\partial z}\left[\mu\left(\frac{\partial w}{\partial x}+\frac{\partial u}{\partial z}\right)\right]$$

$$\rho \frac{\partial^2 w}{\partial t^2} = \frac{\partial}{\partial x}\left[\lambda\left(\frac{\partial u}{\partial x}+\frac{\partial w}{\partial z}\right)+2\mu\frac{\partial w}{\partial z}\right] + \frac{\partial}{\partial x}\left[\mu\left(\frac{\partial w}{\partial x}+\frac{\partial u}{\partial z}\right)\right]$$

WHERE: $u(x, z)$ AND $w(x, z)$ ARE DISPLACEMENTS IN x AND z DIRECTIONS

$\alpha = \sqrt{\frac{\lambda+2\mu}{\rho}}$ IS THE COMPRESSIONAL VELOCITY

$\beta = \sqrt{\frac{\mu}{\rho}}$ IS THE SHEAR VELOCITY

$\rho$ IS THE DENSITY

## FINITE DIFFERENCE APPROXIMATIONS ( EXPLICIT CASE )

SECOND ORDER SPATIAL DERIVATIVES

$$\frac{\partial}{\partial x}\left[\alpha^2(x, z)\frac{\partial}{\partial x}u(x, z, t)\right] = \left\{\alpha^2\left(m+\tfrac{1}{2}, n\right)\left[u(m+1, n, l) - u(m, n, l)\right] - \alpha^2\left(m-\tfrac{1}{2}, n\right)\left[u(m, n, l) - u(m-1, n, l)\right]\right\} \Big/ (\Delta H)^2$$

CROSS PRODUCT SPATIAL DERIVATIVES

$$\frac{\partial}{\partial z}\left[\alpha^2(x, z)\frac{\partial}{\partial x}u(x, z, t)\right] = \left\{\alpha^2(m, n+1)\left[u(m+1, n+1, l) - u(m-1, n+1, l)\right] - \alpha^2(m, n-1)\left[u(m+1, n-1, l) - u(m-1, n-1, l)\right]\right\} \Big/ 4(\Delta H)^2$$

SECOND ORDER TIME DERIVATIVE

$$u(m, n, l+1) = 2u(m, n, l) - u(m, n, l-1) + f\left[\text{Spatial derivatives}\right]$$

WHERE: $\alpha^2\left(m \pm \tfrac{1}{2}, n\right) = \left[\alpha^2(m \pm 1, n) + \alpha^2(m,n)\right] \Big/ 2$

m AND n REFER TO THE x AND z DIRECTION GRID POINTS AND l IS THE TIME STEP

Figure 7.

## PRACTICAL ASPECTS OF EXPLICIT FINITE DIFFERENCE SYNTHETIC SEISMOGRAM CALCULATION

- TWO DIMENSIONAL APPLICATION
- SOURCE GENERATION
- FREE SURFACE BOUNDARY CONDITION
- ABSORBING BOUNDARIES AT EDGES OF MODEL
- STABILITY CONDITION (SMALL TIME STEP)
- ACCURACY CONDITION (SMALL GRID SPACING)
- NUMBER OF TIME STEPS (LENGTH OF SEISMOGRAMS)
- NUMBER OF GRID POINTS
- LARGE COMPUTER TIME AND STORAGE REQUIREMENTS

Figure 8.

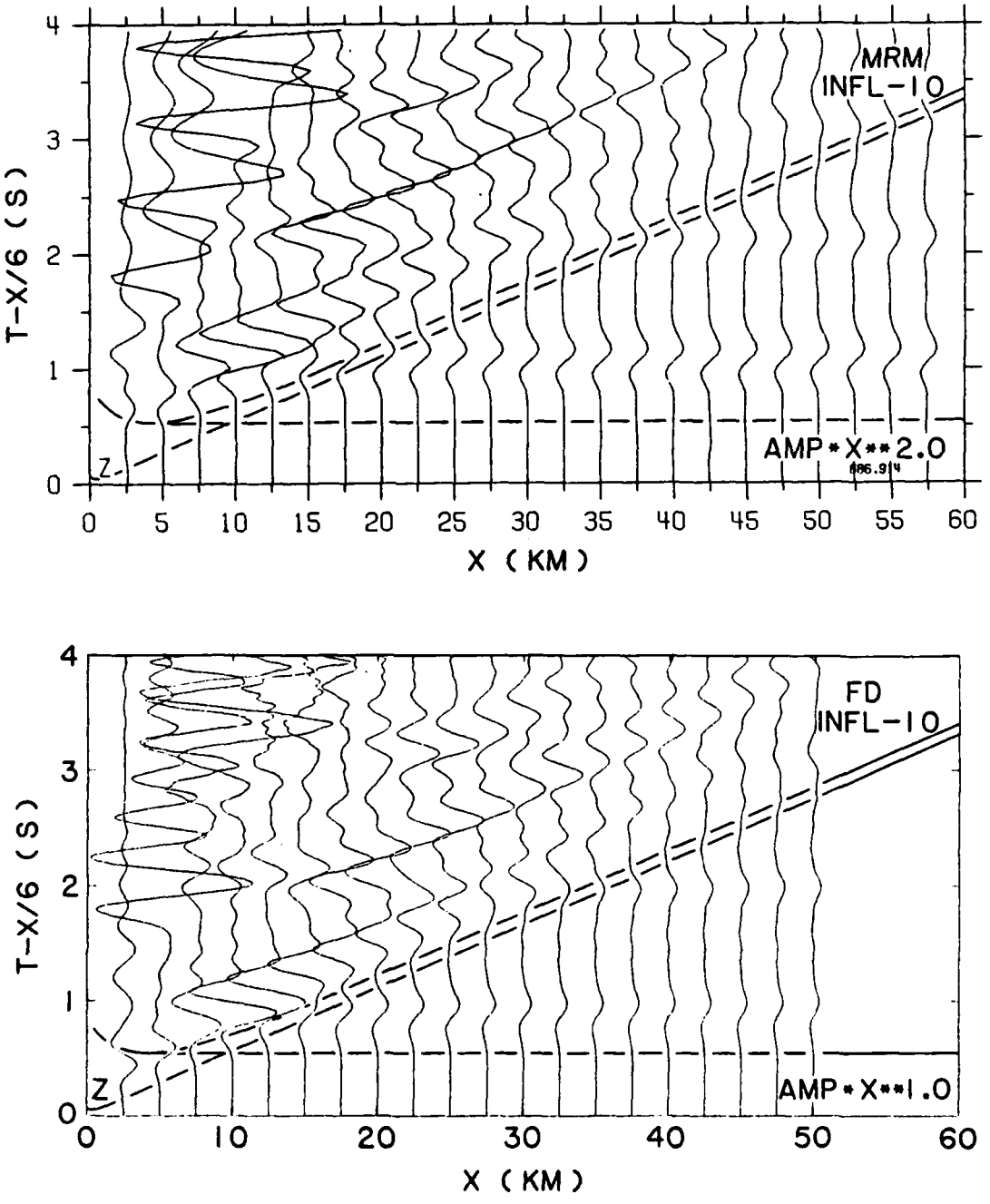
MRM
INFL-10
AMP*X**2.0
Z
T-X/6 (S)
X (KM)
0
1
2
3
4
0
5
10
15
20
25
30
35
40
45
50
55
60
FD
INFL-10
AMP*X**1.0
Z
T-X/6 (S)
X (KM)
0
1
2
3
4
0
10
20
30
40
50
60

Figure 9.

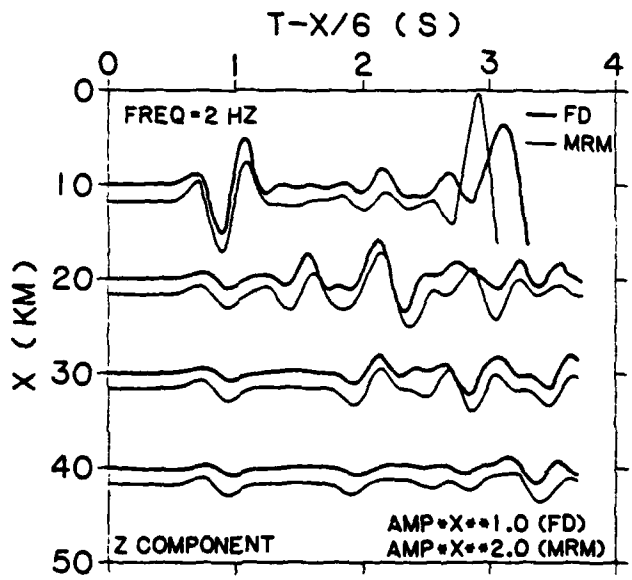


COMPARISON OF FINITE DIFFERENCE (FD) AND MODIFIED REFLECTIVITY METHOD (MRM) SYNTHETICS FOR LAYER OVER HALF SPACE MODEL

Figure 10.

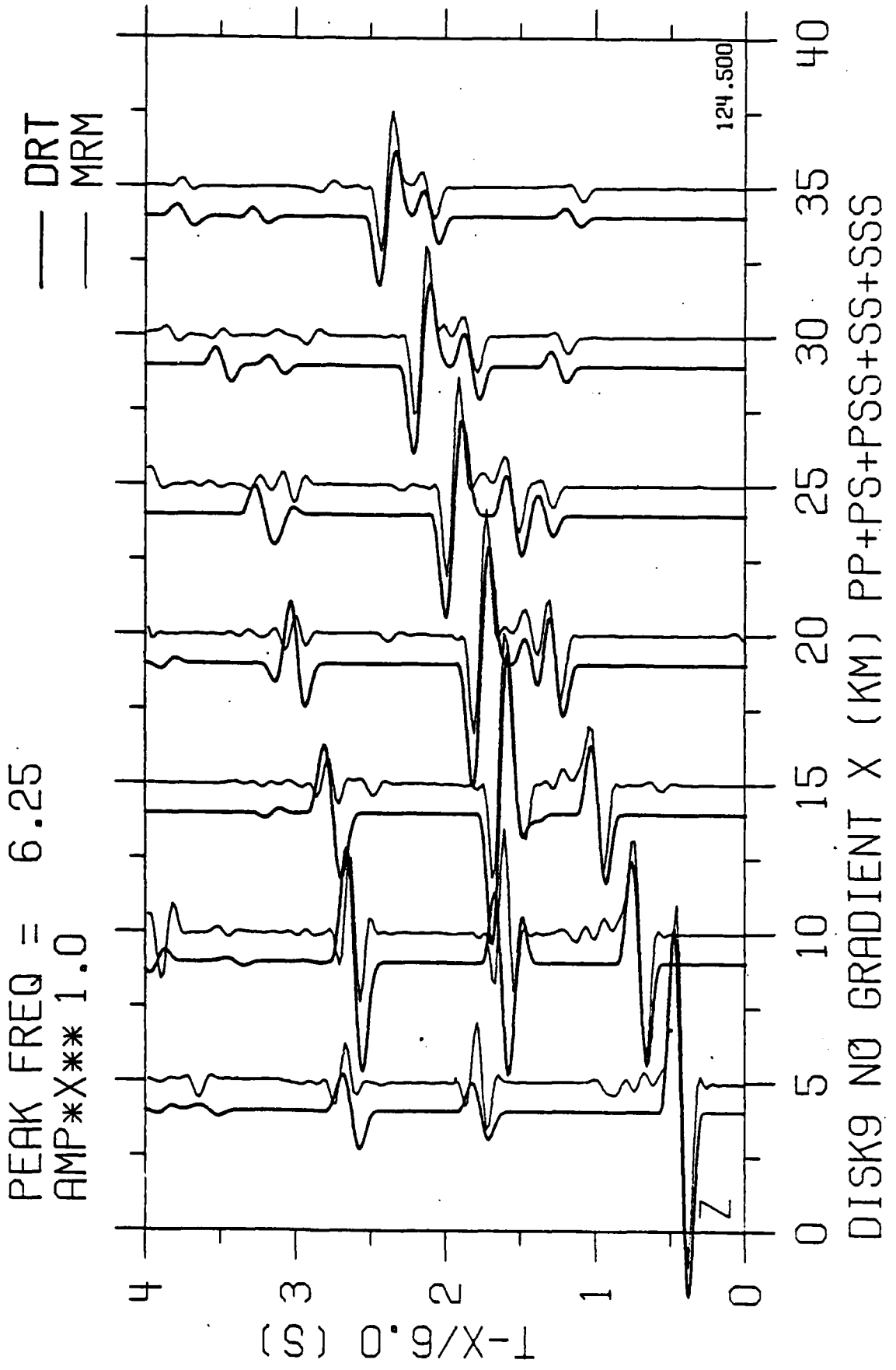
DRT
MRM
PEAK FREQ = 6.25
AMP**X** 1.0
124.500
DISK9 N0 GRADIENT X (KM) PP+PS+PSS+SS+SSS
T-X/6.0 (S)
0
5
10
15
20
25
30
35
40
0
1
2
3
4
Z

Figure 11.

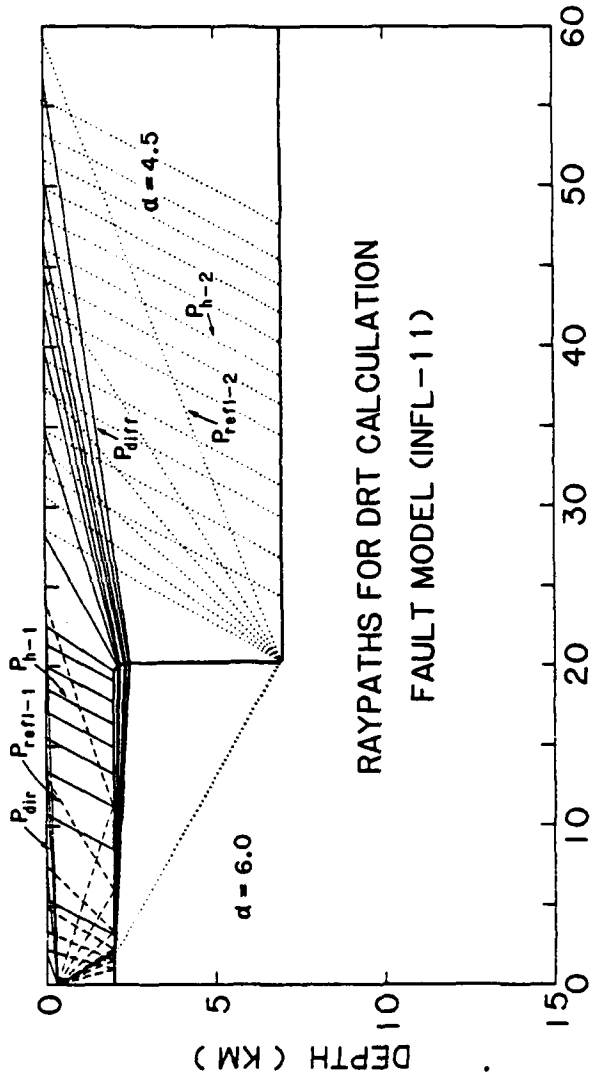
RAYPATHS FOR DRT CALCULATION
FAULT MODEL (INFL-11)
DEPTH (KM)
DISTANCE (KM)
0
5
10
15
0
10
20
30
40
50
60
α = 4.5
α = 6.0
P_dir
P_refl-1
P_h-1
P_diff
P_h-2
P_refl-2

Figure 12.

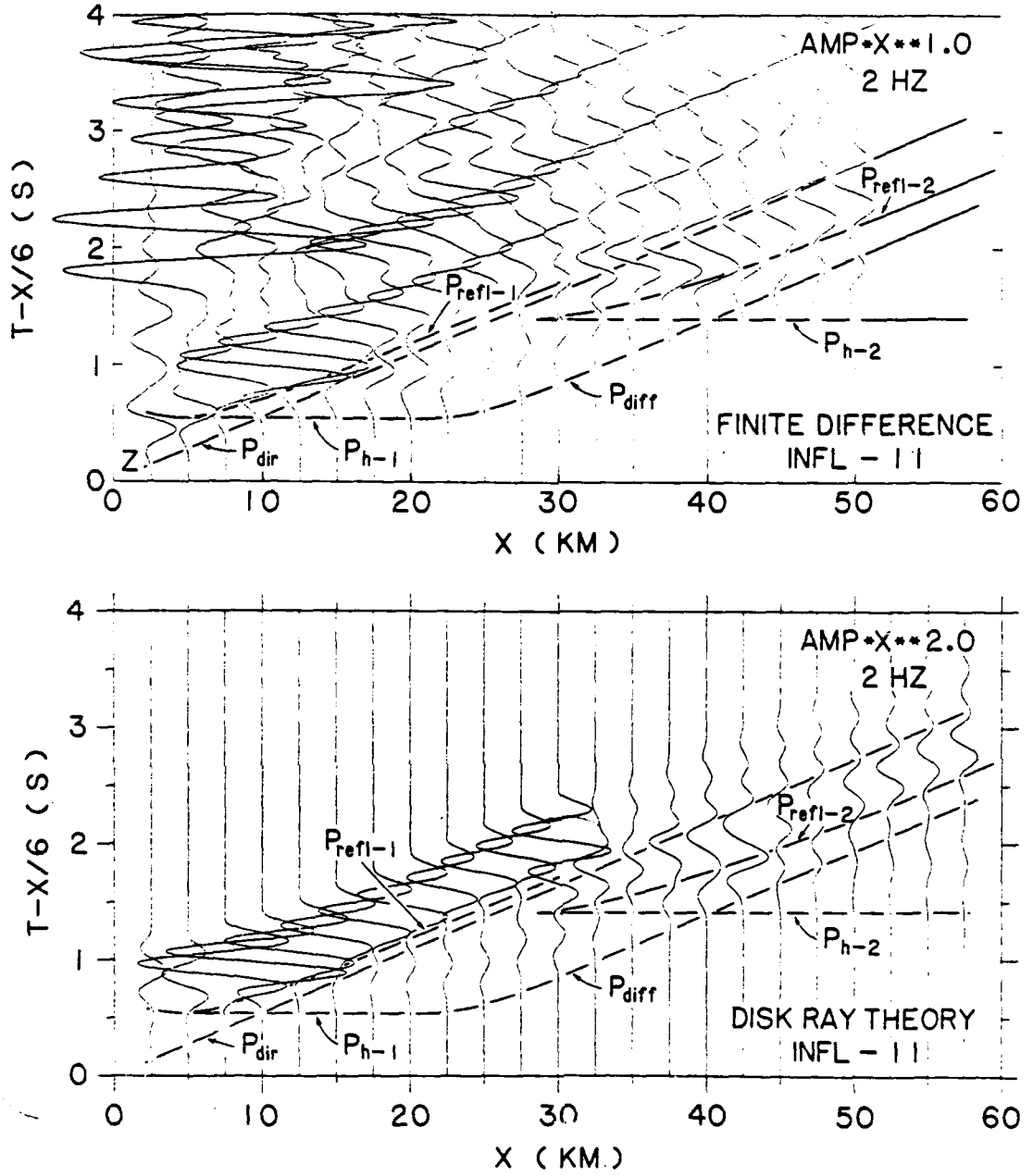
AMP*X**1.0
2 HZ
$P_{refl-2}$
$P_{refl-1}$
$P_{h-2}$
$P_{diff}$
FINITE DIFFERENCE
INFL - 11
Z
$P_{dir}$
$P_{h-1}$
T-X/6 (S)
X (KM)
AMP*X**2.0
2 HZ
$P_{refl-2}$
$P_{refl-1}$
$P_{h-2}$
$P_{diff}$
DISK RAY THEORY
INFL - 11
$P_{dir}$
$P_{h-1}$
T-X/6 (S)
X (KM)

Figure 13.

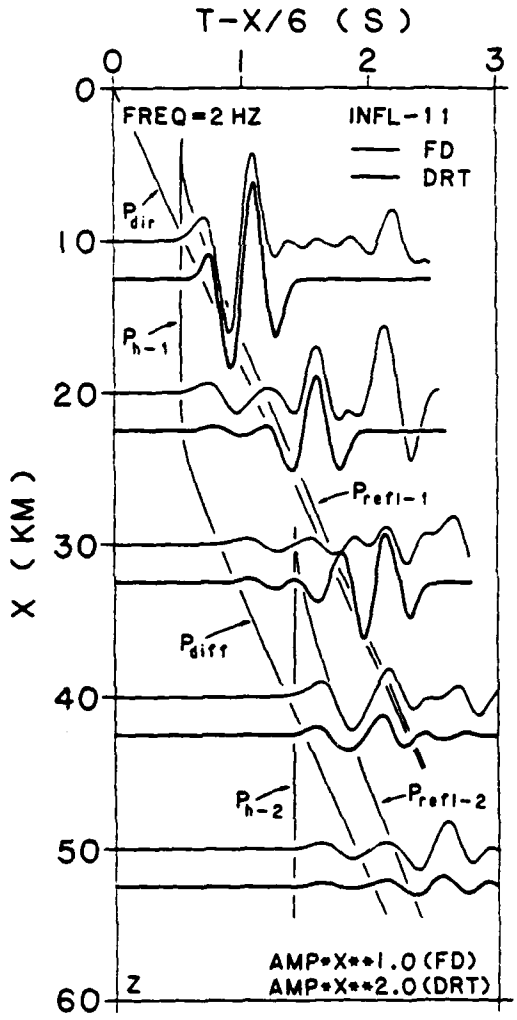


COMPARISON OF FINITE DIFFERENCE (FD) AND DISK RAY THEORY (DRT) SYNTHETICS FOR FAULT MODEL INFL-11

Figure 14.

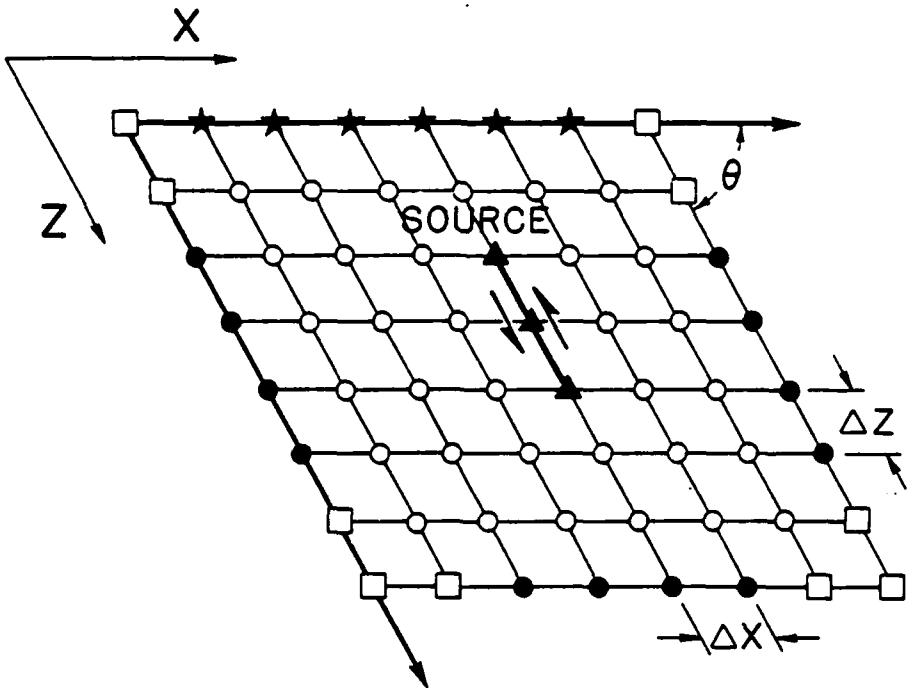


# FINITE DIFFERENCE MODEL iN SKEW COORDINATES

- ○ FULL SECOND ORDER DERIVATIVES
- ● ABSORBING BOUNDARIES, SECOND ORDER PARAXIAL APPROXIMATION
- □ CORNERS, FIRST ORDER PARAXIAL APPROXIMATION
- ★ FREE SURFACE BOUNDARY CONDITION
- ▲ DISLOCATION SOURCE GRID POINTS

Figure 15.

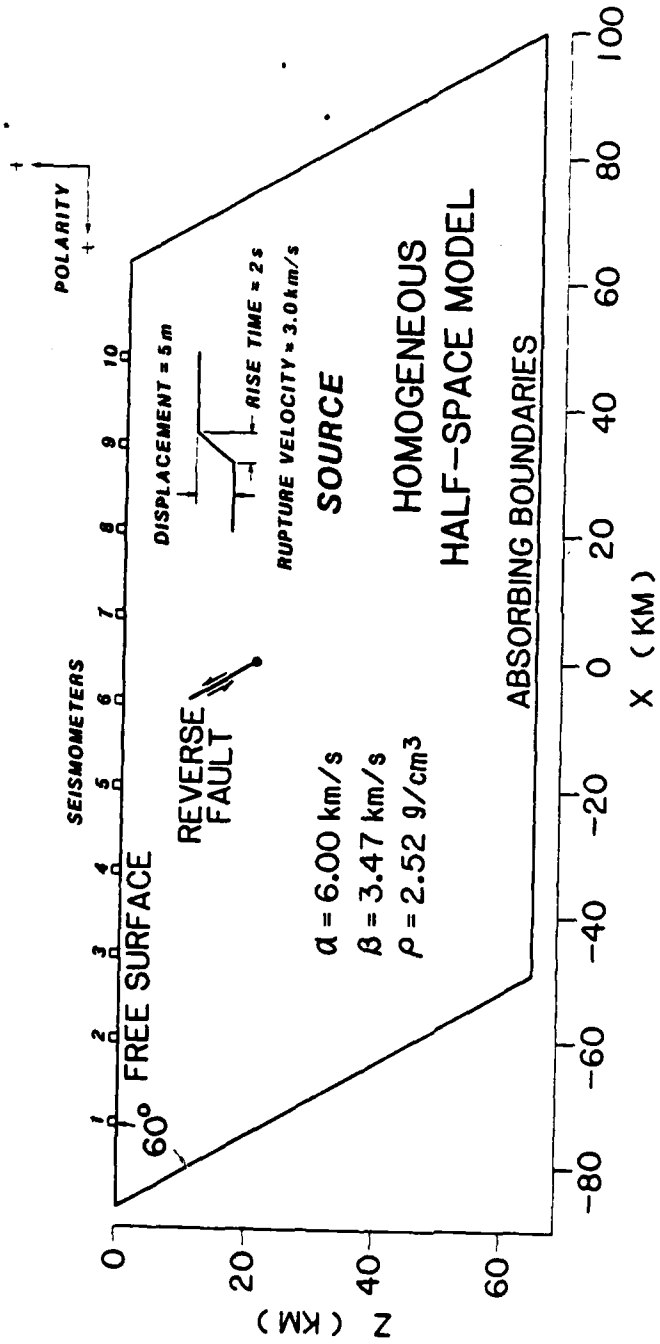
POLARITY
+
-
SEISMOMETERS
1
2
3
4
5
6
7
8
9
10
FREE SURFACE
60°
REVERSE FAULT
DISPLACEMENT = 5 m
RISE TIME = 2 s
RUPTURE VELOCITY = 3.0 km/s
SOURCE
α = 6.00 km/s
β = 3.47 km/s
ρ = 2.52 g/cm³
HOMOGENEOUS
HALF-SPACE MODEL
ABSORBING BOUNDARIES
Z (KM)
0
20
40
60
X (KM)
-80
-60
-40
-20
0
20
40
60
80
100

Figure 16.

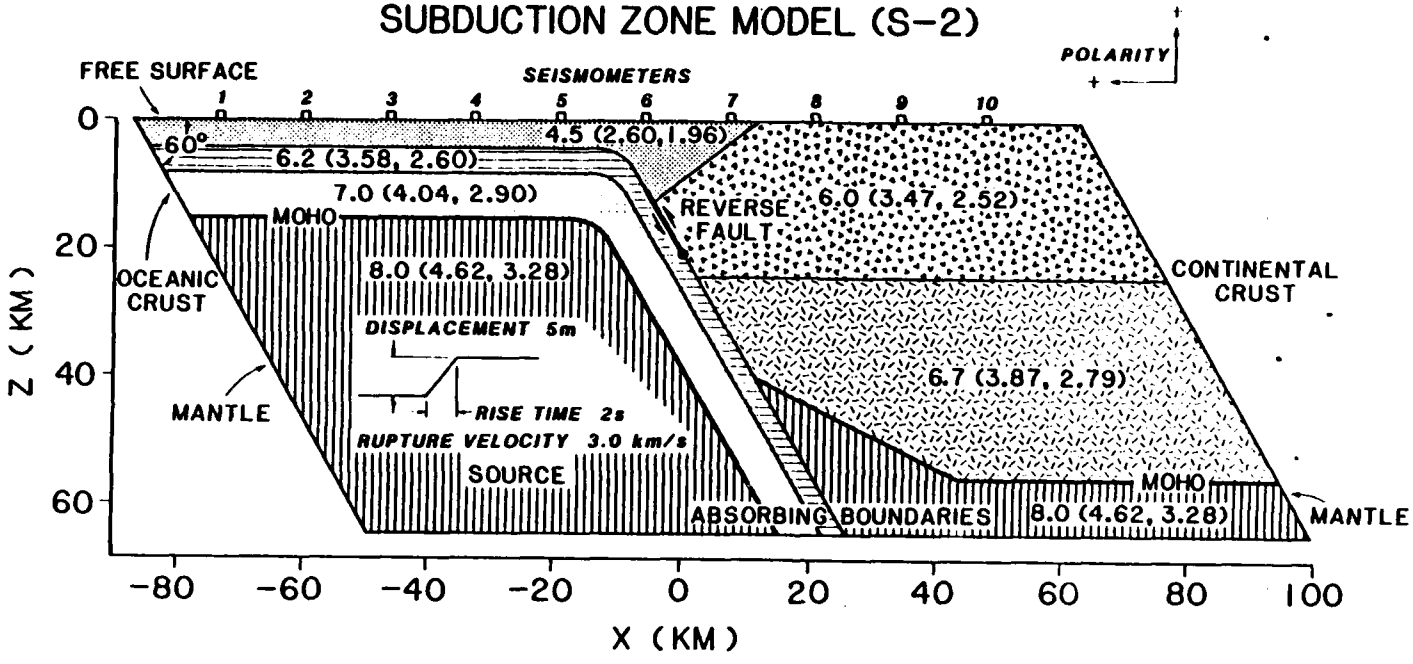
SUBDUCTION ZONE MODEL (S-2)
FREE SURFACE
SEISMOMETERS
1
2
3
4
5
6
7
8
9
10
POLARITY
+
+
0
20
40
60
Z (KM)
60°
4.5 (2.60, 1.96)
6.2 (3.58, 2.60)
7.0 (4.04, 2.90)
MOHO
REVERSE FAULT
6.0 (3.47, 2.52)
CONTINENTAL CRUST
OCEANIC CRUST
8.0 (4.62, 3.28)
DISPLACEMENT 5m
6.7 (3.87, 2.79)
MANTLE
RISE TIME 2s
RUPTURE VELOCITY 3.0 km/s
SOURCE
MOHO
ABSORBING BOUNDARIES
8.0 (4.62, 3.28)
MANTLE
-80
-60
-40
-20
0
20
40
60
80
100
X (KM)

Figure 17.

## EARTHQUAKE SOURCE DESCRIPTIONS FOR FINITE DIFFERENCE SYNTHETIC PROGRAM (SYSMO)

| MODEL | FAULT GEOMETRY | SLIP FUNCTION | SOURCE TIME HISTORY |
|---|---|---|---|
| S-1 A<br>S-2 A | <br>REVERSE FAULT<br>(Rupture Velocity = 3.0 KM/S) | 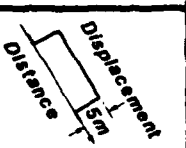 <br>RECTANGULAR WEIGHTING | 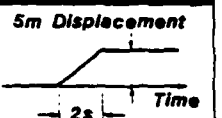 <br>RAMP FUNCTION |
| S-1 B | Same | <br>COSINE BELL WEIGHTING | 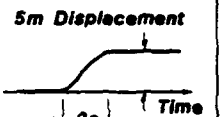 <br>COSINE FUNCTION |
| S-1 C | Same | Same | 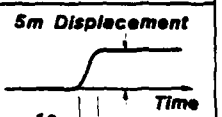 <br>COSINE FUNCTION |

Figure 18.

SEISMIC RAYPATHS FROM A DIPPING FAULT SOURCE FOR A RAMP FUNCTION DISPLACEMENT IN A HOMOGENEOUS HALF-SPACE MODEL

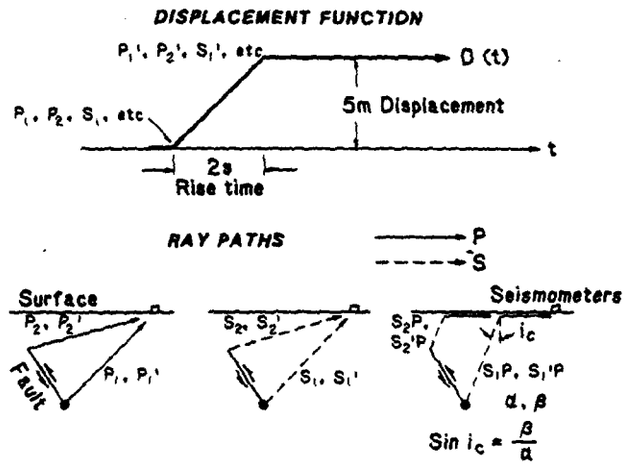


Figure 19.

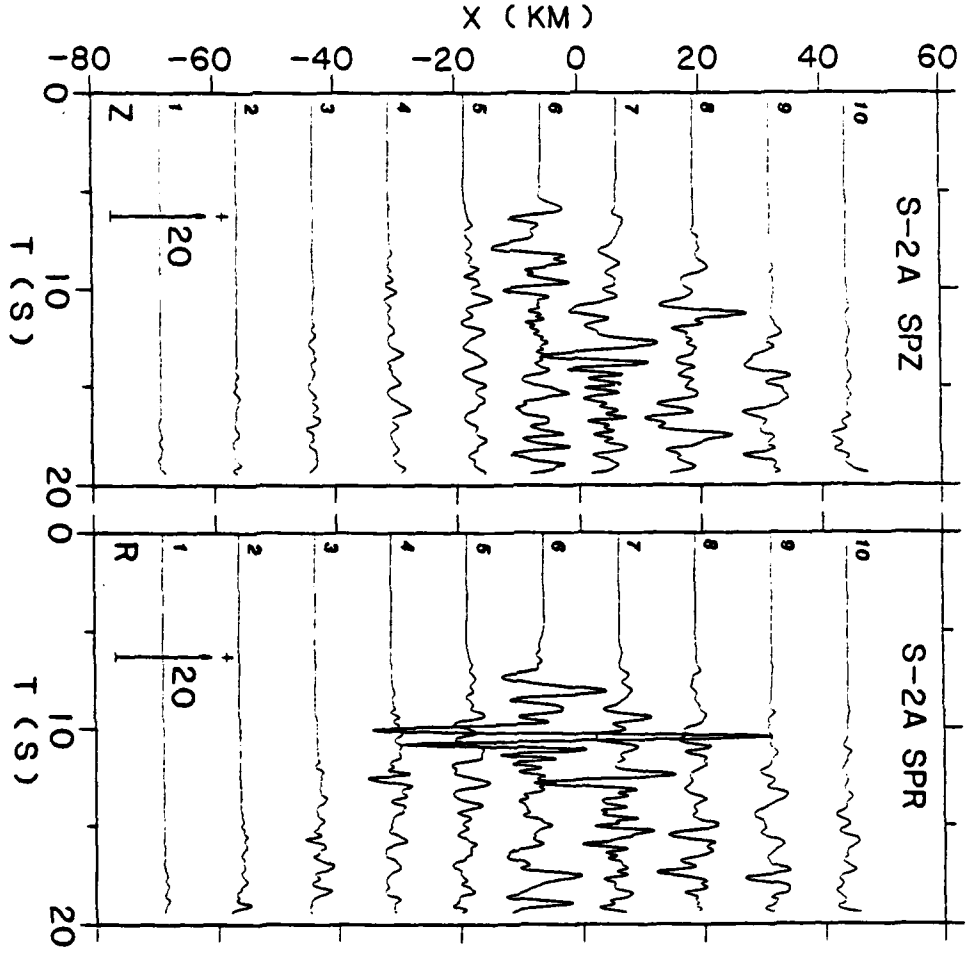
X (KM)
-80
-60
-40
-20
0
20
40
60
Z
R
20
T (S)
0
10
20
S-2A SPZ
S-2A SPR
1
2
3
4
5
6
7
8
9
10

Figure 20.

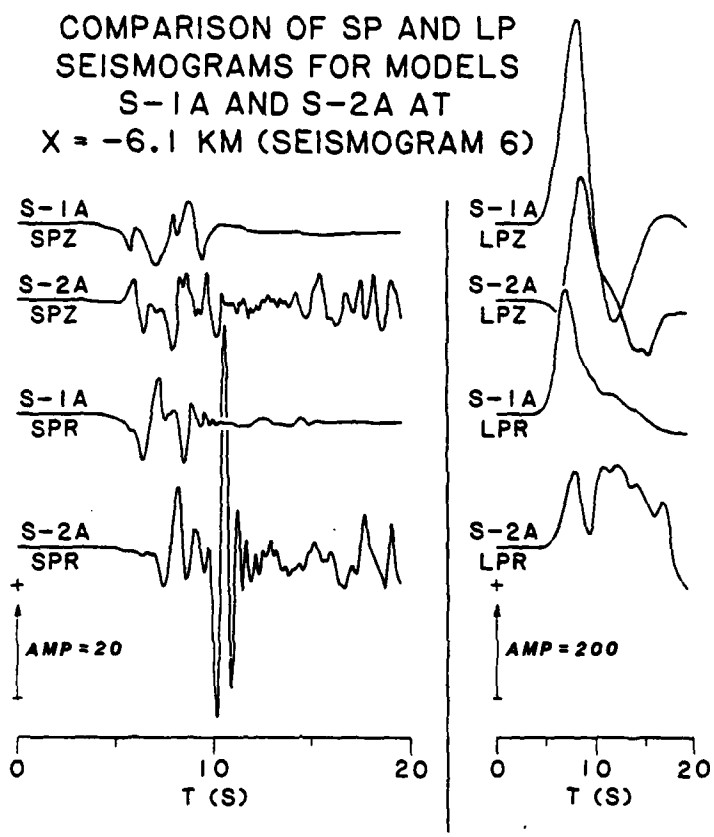
COMPARISON OF SP AND LP
SEISMOGRAMS FOR MODELS
S-1A AND S-2A AT
X = -6.1 KM (SEISMOGRAM 6)
S-1A
SPZ
S-2A
SPZ
S-1A
SPR
S-2A
SPR
AMP = 20
0
10
20
T (S)
S-1A
LPZ
S-2A
LPZ
S-1A
LPR
S-2A
LPR
AMP = 200
0
10
20
T (S)

Figure 21.

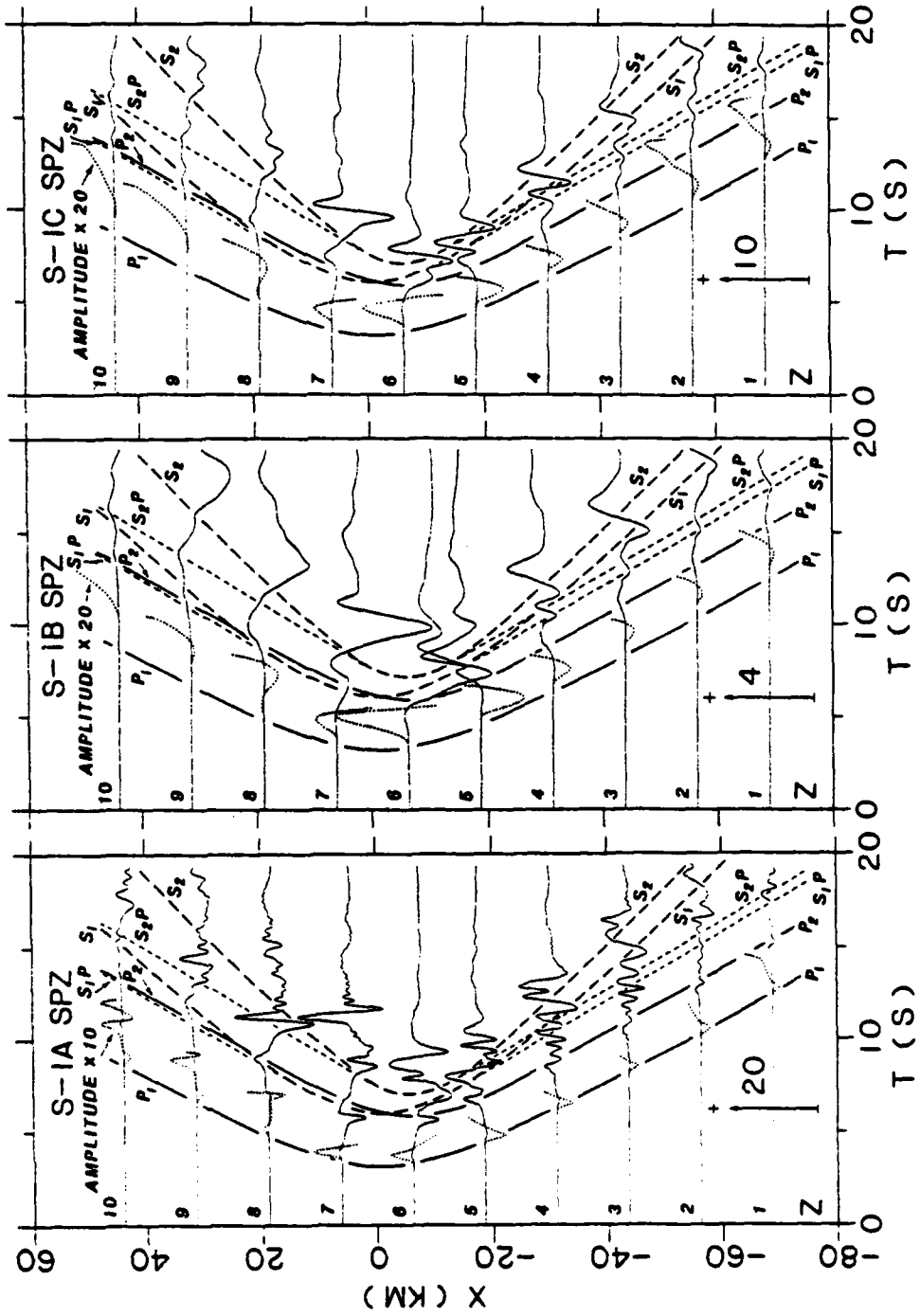
S-IA SPZ
AMPLITUDE X 10
S-IB SPZ
AMPLITUDE X 20
S-IC SPZ
AMPLITUDE X 20
P1
P2
S1
S2
S1P
S2P
Z
20
4
10
T (S)
X (KM)
60
40
20
0
-20
-40
-60
-80

Figure 22.

SCALAR WAVE EQUATION

$$\frac{\partial^2}{\partial t^2} U = C_0^2 \left( \frac{\partial^2}{\partial x^2} + \frac{\partial^2}{\partial z^2} \right) U$$

EXPLICIT FINITE DIFF FORM

$$\delta_t^2 U_{ij}^n = p^2 ( \delta_x^2 + \delta_z^2 ) U_{ij}^n$$

IMPLICIT FINITE DIFF FORM

$$\delta_t^2 U_{ij}^n = \frac{p^2}{3} ( \delta_x^2 + \delta_z^2 ) ( U_{ij}^{n+1} + U_{ij}^n + U_{ij}^{n-1} )$$

WHERE: $U_{ij}^n$ = Pressure at: time step = n, x coord = i, z coord = j

$$p = C_0 \frac{\Delta t}{\Delta x}$$

Second Order Difference Operators:

$$\delta_x^2 U_{ij}^n = U_{i+1\,j}^n - 2U_{ij}^n + U_{i-1\,j}^n$$

$$\delta_z^2 U_{ij}^n = U_{i\,j+1}^n - 2U_{ij}^n + U_{i\,j-1}^n$$

$$\delta_t^2 U_{ij}^n = U_{ij}^{n+1} - 2U_{ij}^n + U_{ij}^{n-1}$$

Figure 23.

## EXPLICIT FINITE DIFF FORM

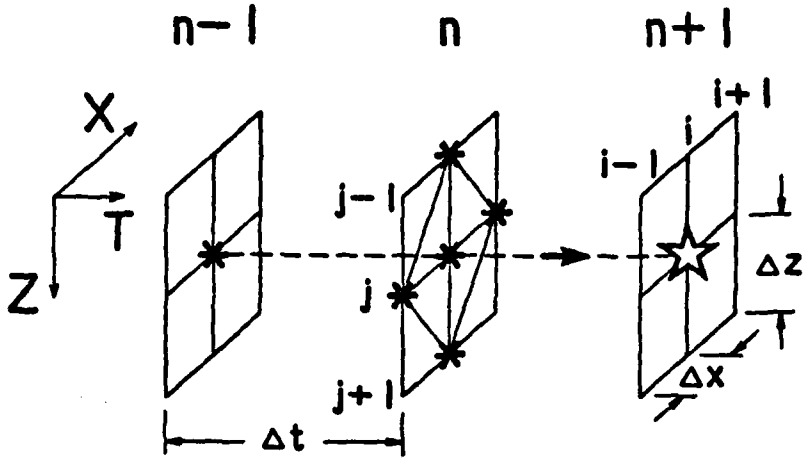


$$U_{ij}^{n+1} - 2U_{ij}^{n} + U_{ij}^{n-1} = p^2(\delta_x^2 + \delta_z^2)U_{ij}^{n}$$

## IMPLICIT FINITE DIFF FORM

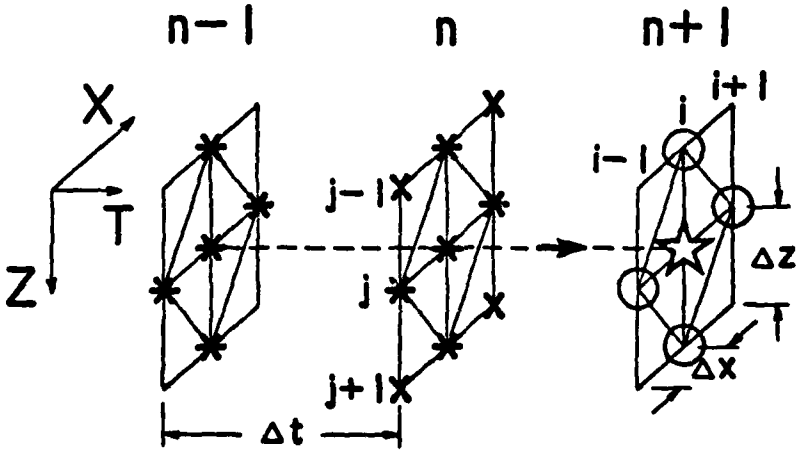


$$U_{ij}^{n+1} - 2U_{ij}^{n} + U_{ij}^{n-1} = \frac{p^2}{3}(\delta_x^2 + \delta_z^2)(U_{ij}^{n+1} + U_{ij}^{n} + U_{ij}^{n-1})$$

Figure 24.

## FIVE POSSIBLE FINITE DIFFERENCE METHODS FOR SCALAR WAVE EQUATION

**Explicit** Stable for $p < 0.7$ (Alford, Kelly and Boore, 1974)

$$U_{ij}^{n+1} - 2U_{ij}^{n} + U_{ij}^{n-1} = p^2 \, (\delta_x^2 + \delta_z^2) U_{ij}^{n}$$

**Implicit** Unconditionally Stable (Emerman, Schmidt and Stephen, 1982)

$$U_{ij}^{n+1} - 2U_{ij}^{n} + U_{ij}^{n-1} = \frac{p^2}{3} \, (\delta^2 + \delta_z^2)(U_{ij}^{n+1} + U_{ij}^{n} + U_{ij}^{n-1})$$

**Implicit** Stability Dependant on $\eta$ (Lees, 1962)

$$(1 - \eta \, p^2 \delta_x^2)(1 - \eta p^2 \delta_z^2)(U_{ij}^{n+1} - 2U_{ij}^{n} + U_{ij}^{n-1}) = p^2 \, (\delta_x^2 + \delta_z^2) U_{ij}^{n}$$

**Implicit** Stable for $p < 0.7$ High Accuracy (Fairweather and Mitchell, 1965)

$$[1 + \tfrac{1}{12}(1 - p^2) \, \delta_x^2 \,][1 + \tfrac{1}{12}(1 - p^2) \, \delta_z^2 \,](U_{ij}^{n+1} - 2U_{ij}^{n} + U_{ij}^{n-1}) = p^2 [(\delta_x^2 + \delta_z^2) + \tfrac{1}{6} \, \delta_x^2 \, \delta_z^2 \,] U_{ij}^{n}$$

**Implicit** Unconditionally Stable Intermediate Accuracy (Samarskii, 1964)

$$[1 + \tfrac{1}{12}(1 - 6p^2) \, \delta_x^2 \,][1 + \tfrac{1}{12}(1 - 6p^2) \, \delta_z^2 \,](U_{ij}^{n+1} - 2U_{ij}^{n} + U_{ij}^{n-1}) = p^2 [(\delta_x^2 + \delta_z^2) + \tfrac{1}{6} \, \delta_x^2 \, \delta_z^2 \,] U_{ij}^{n}$$



Figure 25.

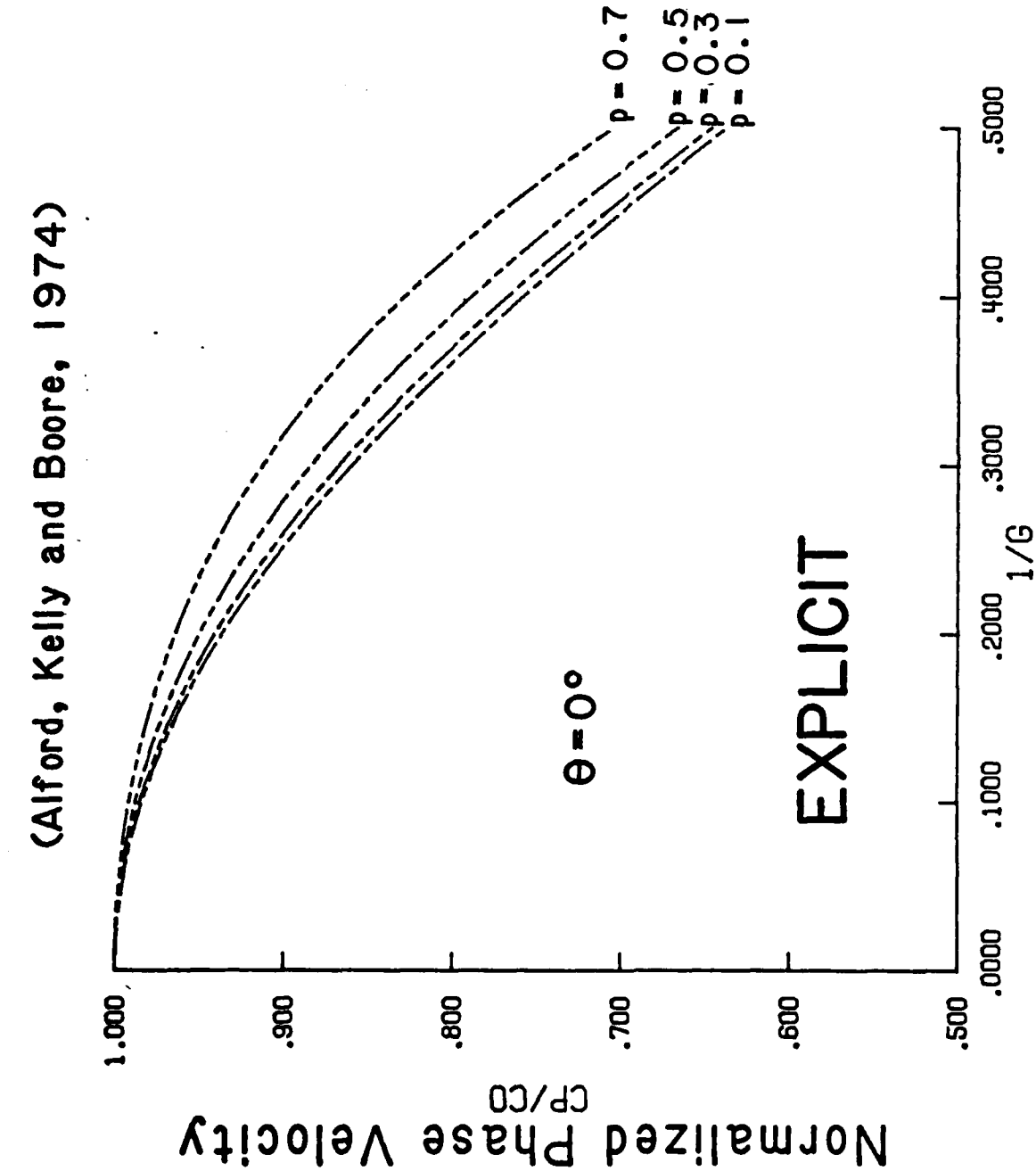
(Alford, Kelly and Boore, 1974)
Normalized Phase Velocity
CP/CO
1.000
.900
.800
.700
.600
.500
θ=0°
EXPLICIT
p = 0.7
p = 0.5
p = 0.3
p = 0.1
.0000
.1000
.2000
.3000
.4000
.5000
1/G
Wavelengths per Grid Point

Figure 26.

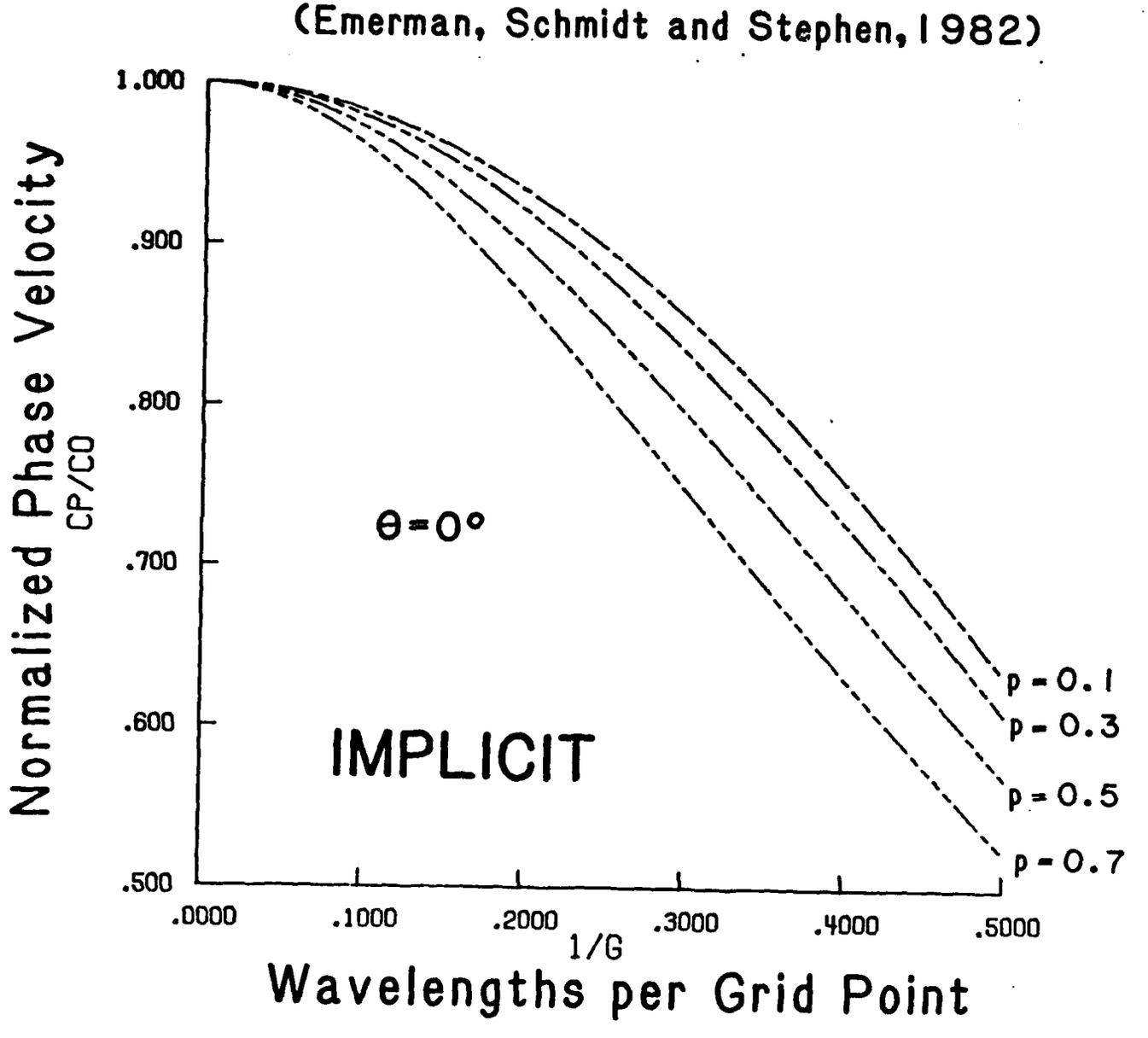
(Emerman, Schmidt and Stephen, 1982)
Normalized Phase Velocity
CP/CO
1.000
.900
.800
.700
.600
.500
θ=0°
IMPLICIT
p = 0.1
p = 0.3
p = 0.5
p = 0.7
.0000
.1000
.2000
.3000
.4000
.5000
1/G
Wavelengths per Grid Point

Figure 27.

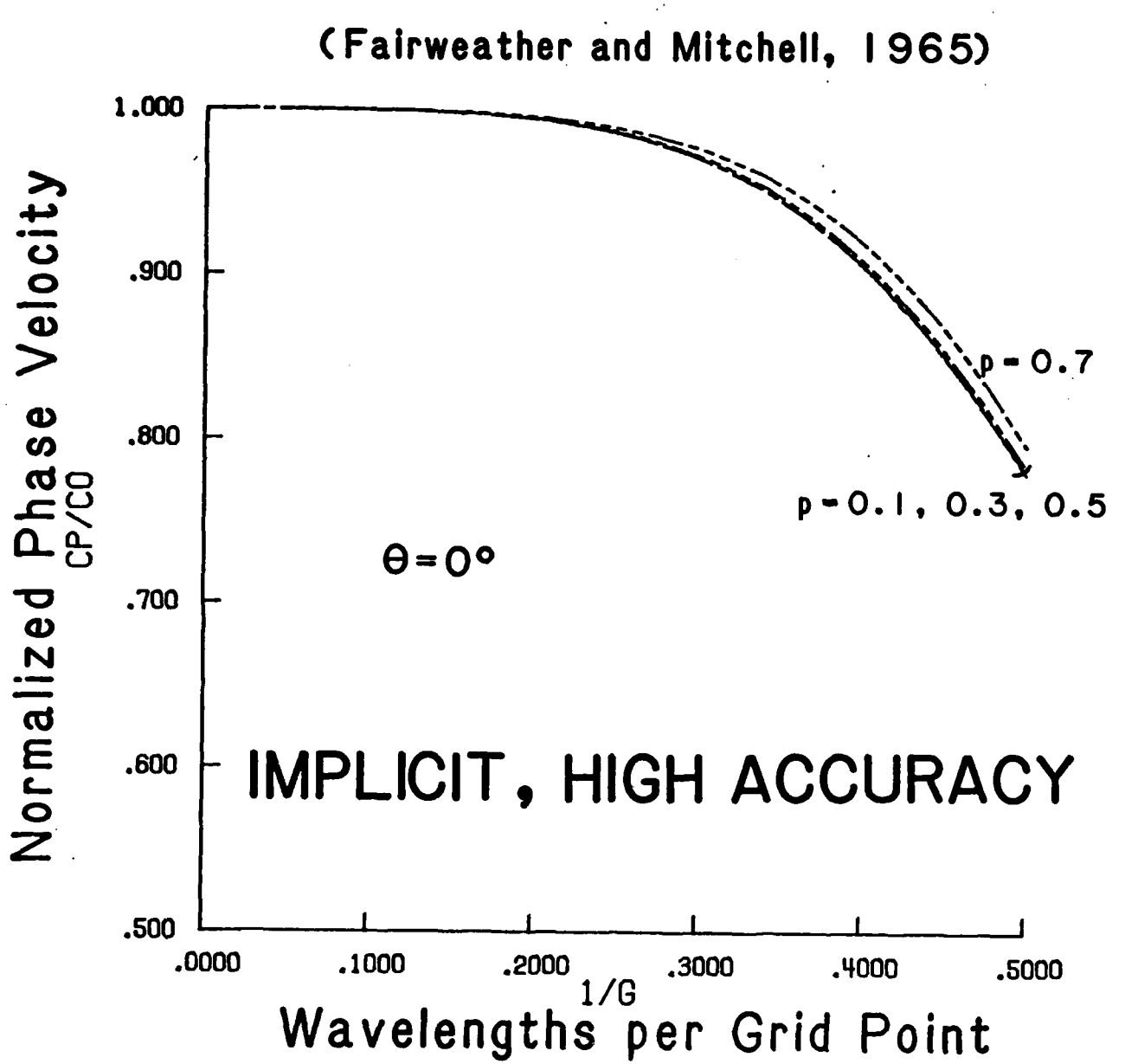
(Fairweather and Mitchell, 1965)
1.000
.900
.800
.700
.600
.500
Normalized Phase Velocity
CP/CO
p = 0.7
p = 0.1, 0.3, 0.5
θ = 0°
IMPLICIT, HIGH ACCURACY
.0000
.1000
.2000
.3000
.4000
.5000
1/G
Wavelengths per Grid Point

Figure 28.

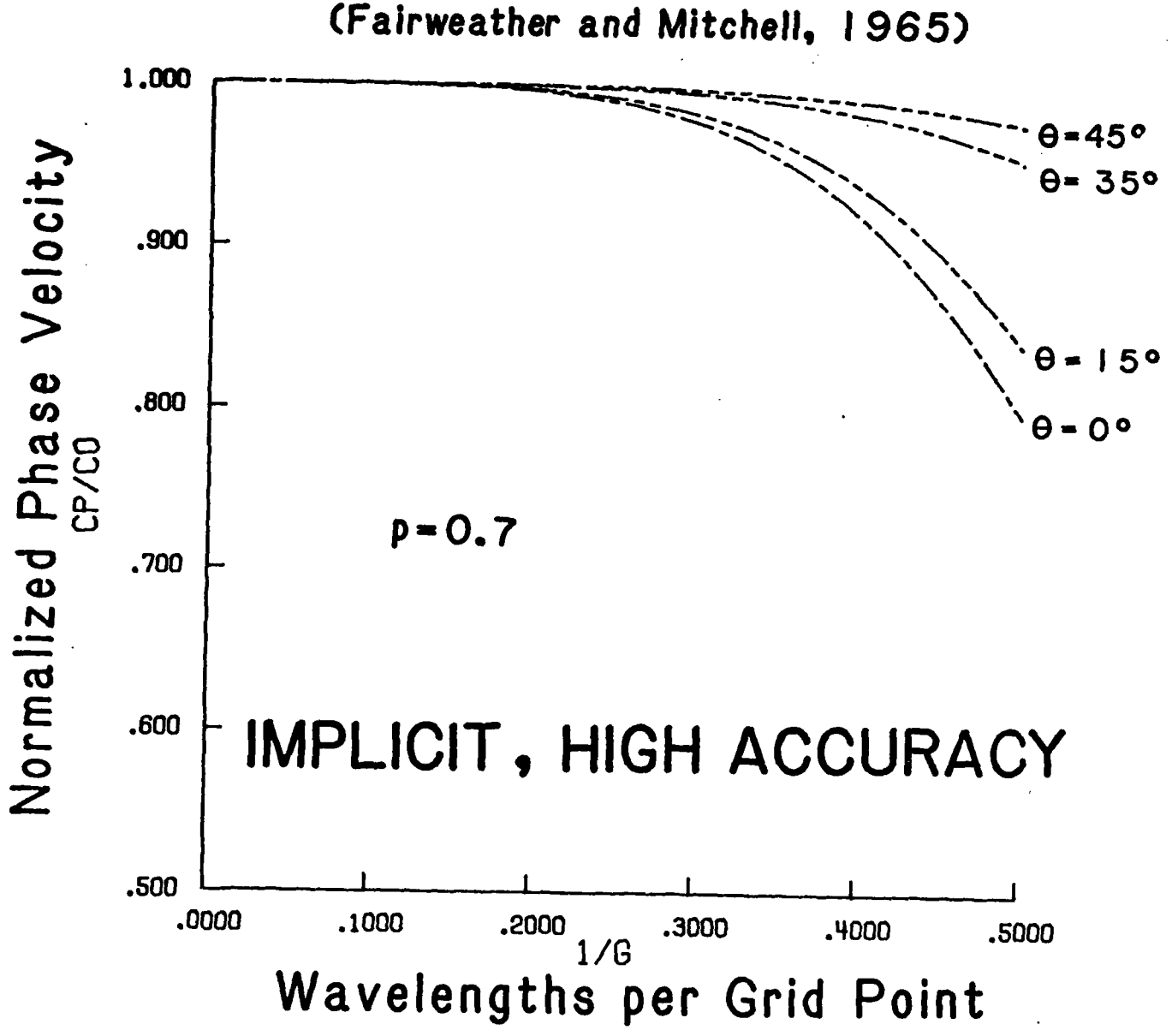
(Fairweather and Mitchell, 1965)
Normalized Phase Velocity
CP/CO
1.000
.900
.800
.700
.600
.500
θ=45°
θ= 35°
θ= 15°
θ= 0°
p=0.7
IMPLICIT, HIGH ACCURACY
.0000
.1000
.2000
.3000
.4000
.5000
1/G
Wavelengths per Grid Point

Figure 29.

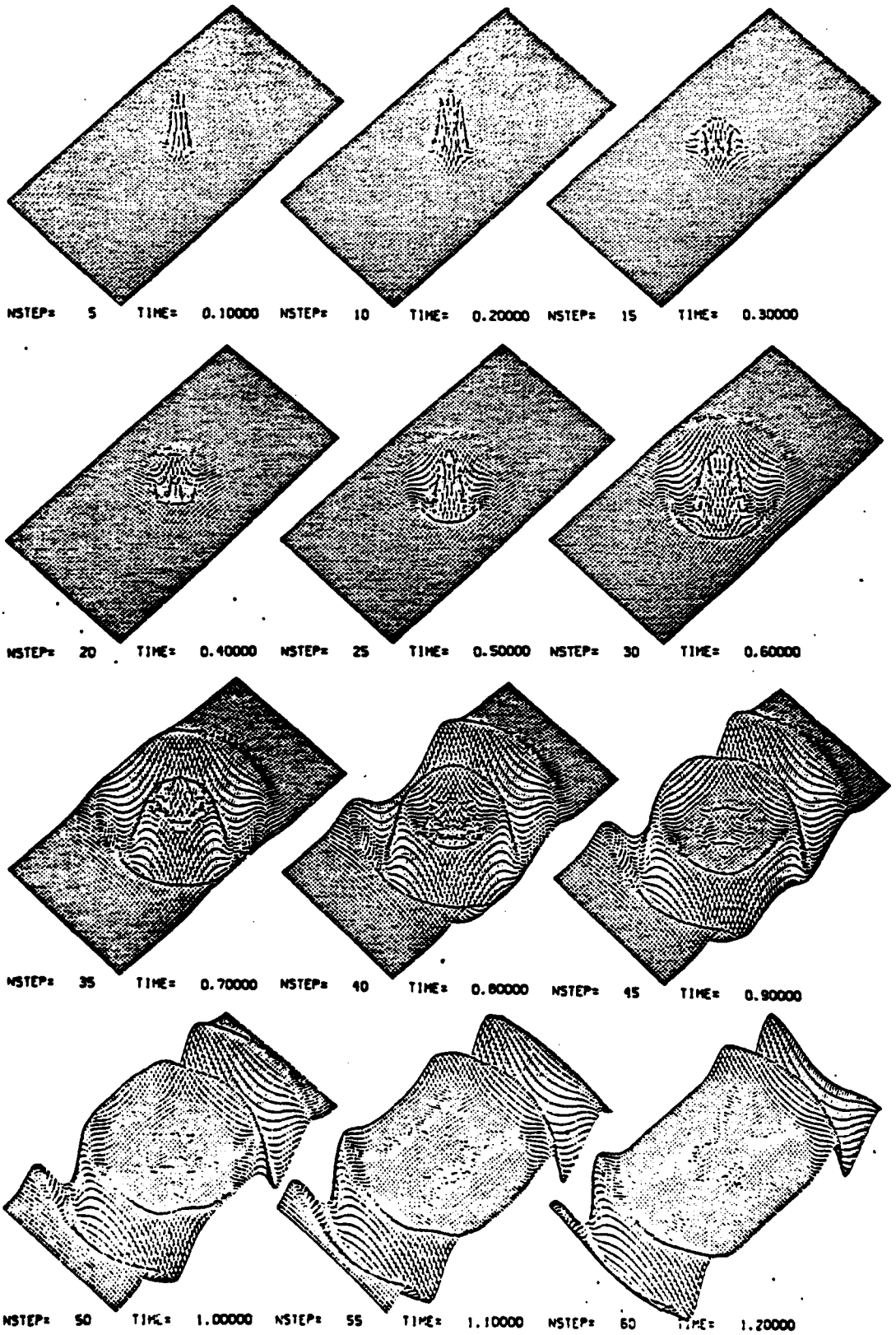
NSTEP= 5 TIME= 0.10000 NSTEP= 10 TIME= 0.20000 NSTEP= 15 TIME= 0.30000
NSTEP= 20 TIME= 0.40000 NSTEP= 25 TIME= 0.50000 NSTEP= 30 TIME= 0.60000
NSTEP= 35 TIME= 0.70000 NSTEP= 40 TIME= 0.80000 NSTEP= 45 TIME= 0.90000
NSTEP= 50 TIME= 1.00000 NSTEP= 55 TIME= 1.10000 NSTEP= 60 TIME= 1.20000

Figure 30.

# DISTRIBUTION LIST

Chief of Naval Research
Department of the Navy
800 North Quincy Street
Arlington, Virginia 22217
- Code 100C1 (1)
- Code 460 (1)
- Code 463 (5)
- Code 480 (1)
- Code 420 (1)

ONR Resident Representative
Ohio State Univ. Research Center
1314 Kinnear Road
Columbus, OH 43212 (1)

Director
Naval Research Laboratory
Code 2627
Washington, DC 20375 (6)

Director
Defense Advanced Research
Projects Agency
1400 Wilson Boulevard
Arlington, VA 22209 (1)

Office of Naval Research
Branch Office/Chicago
536 South Clark St.
Chicago, IL 60605 (1)

Director, Environmental Sciences Directorate
Geophysical Sciences Division
Office of Naval Research
800 North Quincy Street
Arlington, VA 22217 (1)

Air Force Office of Scientific Research
Department of the Air Force
Directorate of Physics (MPG)
Building 410
Bolling Air Force Base
Washington, DC 20332 (1)

Army Research Office
Department of the Army
Geosciences Division
Box 12211
Research Triangle Park, NC 27709 (1)

Defense Technical Information Center
Building 5
Cameron Station
Alexandria, VA 22314 (12)

Procuring Contracting Officer, Code 614B:DAW
Office of Naval Research
Department of the Navy
800 North Quincy Street
Arlington, VA 22217 (1)

# SUPPLEMENTARY DISTRIBUTION LIST

Division of Sponsored Programs
Purdue University
West Lafayette, IN 47907 (1)

Dr. Robert B. Smith
Dept. of Geology & Geophysics
University of Utah
Salt Lake City, UT 84112 (1)

Dr. John Kuo
Henry Krumb School of Mines
Columbia University
New York, NY 10027 (1)

Dr. G.R. Keller
Dept. of Geological Sciences
University of Texas, El Paso
El Paso, TX 79968 (1)

Dr. Ken Olsen
LASL, Group G-7
MS 676
PO Box 1663
Los Alamos, NM 87545 (1)

Dr. Mark Odegard
Dept. of Physics
New Mexico State University
Las Cruces, NM 88003 (1)

Dr. Robert E. Houtz
Lamont-Doherty Geological Obs.
Columbia University
New York, NY 10029 (1)

Dr. John G. Heacock
Earth Physics Program, Code 463
Office of Naval Research
Arlington, VA 22217

Dr. R.F. Obrochta
Office of Naval Research
800 N. Quincy Street
Arlington, VA 22217 (1)

Dr. Murray MacDonald
Code 425
Geology & Geophysics
Office of Naval Research
Bay St. Louis, MS 39522 (1)

# APPENDIX

## AN EXAMPLE OF TWO-DIMENSIONAL SYNTHETIC SEISMOGRAM MODELING

Chao Sheng Chiang and Lawrence W. Braile

Department of Geosciences
Purdue University
West Lafayette, IN 47907

June 1, 1983

## ABSTRACT

Synthetic seismograms for laterally inhomogeneous velocity and Q structures can be calculated by the disk ray theory (DRT) method. Ray-tracing through the model provides travel-time, distance, slowness and ray amplitude data which are combined to synthesize seismic record sections by DRT. The amplitude factors include geometrical spreading, attenuation due to $Q^{-1}$, reflection and transmission coefficients and the free surface conversion coefficient. Comparison of DRT synthetic seismograms with those calculated by the reflectivity method for a layer over a half space model shows excellent agreement in both amplitude and waveform character of all arrivals. Direct, reflected, P to S converted, multiply reflected and head waves may be synthesized by the DRT method. In an application of two-dimensional synthetic seismogram modeling using the DRT method, synthetic seismogram record sections were calculated for a complicated geologic model of the crust in the eastern Snake River Plain, Idaho and compared with observed seismic data. In this application, we find that a small modification of the Snake River Plain velocity model which was interpreted from travel-time data produces seismograms which compare well with the amplitude and waveform character of the observed seismograms.

# INTRODUCTION

Modern crustal seismic refraction and reflection data recorded at relatively small station spacings and of improved quality result in an increased need for two-dimensional synthetic seismogram modeling techniques for interpretation. Both wave-theoretical and ray-theoretical methods have been used for the calculation of synthetic seismograms. Wave methods are generally restricted to one-dimensional velocity models, although finite-element and finite-difference techniques allow calculation in two- and three-dimensional structures. In general, wave-theoretical techniques applied to two-dimensional synthetic seismogram calculations provide highly accurate results but are limited in their practical application due to the extensive cost and computer resources required for their calculation. In contrast, ray-theoretical methods provide only approximate calculations and are limited in their ability to simulate wave propagation effects, but are computationally efficient. In this paper, we briefly describe a modification of the disk-ray theory method (Wiggins, 1976) for calculation of synthetic seismograms in two-dimensional velocity structures and present an example of its application to modeling of a complex geologic model in the eastern Snake River Plain area of southern Idaho. The method is reasonably accurate, is efficient to use for modeling purposes, and is capable of calculating seismograms for complex two-dimensional geologic structures.

A variety of synthetic seismogram modeling techniques have been developed for application to laterally inhomogeneous velocity structures. Cerveny _et al_. (1977) and Cerveny (1979) present a theoretical discussion and results of model studies of asymptotic ray theory (ART) calculations of the amplitudes of seismic waves propagating through an inhomogeneous velocity structure approximating the waves by a series of rays. McMechan

and Mooney (1980) described a modified version of ART and showed an application to modeling of observed crustal seismic data for the Imperial Valley, California. Hong and Helmberger (1978) have utilized a ray theory method known as glorified optics to compute synthetic seismograms for primary and multiple reflections for some homogeneous layer models including non-planar boundaries. Frazer and Phinney (1980) have described the theoretical background for a generalized phase integral method which can be applied to generation of synthetic seismograms in laterally inhomogeneous media. Wiggins (1976) and Wiggins and Madrid (1974) have developed a ray method for the generation of synthetic seismograms in which the effects of wave propagation are simulated by individual rays in which the propagation can be thought of as consisting as 'disks' of energy traveling along the raypath. Each disk, which is perpendicular to the raypath, intersects the surface and affects an area surrounding the point of emergence of the ray. Chapman (1976) described a first motion approximation which is formally equivalent to the disk ray theory technique.

All of the above mentioned techniques are based on ray-theoretical solutions to the elastic wave equation in two-dimensional media. They provide only approximate solutions for particular wave propagation phenomena and are limited in their ability to simulate wave propagation for all types of wave motion and under all geometrical conditions of velocity structure. For example, it is well known that ray theoretical techniques are inaccurate in the area of a caustic or turning point of the seismic rays and have difficulty in the generation of pure head waves. Furthermore, ray techniques are generally limited to body wave propagation problems. More exact wave propagation synthetic seismogram techniques generally involve a direct numerical solution to the elastic wave equation in two-dimensions. Finite difference approximations for this purpose have been used by Boore (1972), Alford et al. (1974) and Kelly et al. (1976)

and finite element methods are described by Smith (1975). Because these techniques represent complete solutions to the wave equation, the finite difference and finite element synthetic seismogram methods are accurate and provide complete seismograms including all types of wave phenomena in both homogeneous and inhomogeneous velocity structures. However, large requirements of computer time and storage for these techniques preclude their use for routine modeling of two-dimensional seismic wave propagation.

## DISK RAY THEORY METHOD

The disk ray theory (DRT) method that we have employed follows the theory of Wiggins and Madrid (1974) and Wiggins (1976). They presented a theoretical discussion of the DRT method based on ray approximations to wave propagation in laterally homogeneous media and pointed out the possibility of utilizing such techniques for laterally inhomogeneous media where ray tracing results would provide the necessary travel time and amplitude information for constructing DRT synthetic seismograms. The DRT method that we have utilized is briefly described below. For a discussion of the theory of the DRT method the reader is referred to Wiggins and Madrid (1974) and Wiggins (1976). The ray tracing data required for DRT synthetic seismogram synthesis follows the ART techniques of Cerveny and Ravindra (1971) and Cerveny et al. (1977).

The first step in DRT synthesis for two-dimensional wave propagation is to calculate travel-time and amplitude factors for seismic raypaths propagating for phases of interest through the velocity structure. For this purpose, we utilize the 'shooting method' of ray tracing in which rays are traced by iterative application of the generalized Snell's Law through the two-dimensional velocity structure from a source location given an initial angle of incidence. The ray may refract or reflect

at boundaries and may include propagation through homogeneous or vertically and laterally inhomogeneous layers. The velocity structure in our models is given by layers of constant or slowly varying seismic velocity separated by irregular interfaces. Alternatively a continuously varying velocity structure with vertical and lateral gradients can be approximated by a two-dimensional grid of seismic wave velocities. Attenuation factors ($Q^{-1}$) are also given for the model. The seismic velocity model utilized employs a flat earth convention and thus we provide for small positive velocity gradients within homogeneous layers to simulate the effects of earth curvature according to the earth flattening transformation (Aki and Richards, 1980, p. 463-465). Using only this small positive velocity gradient within homogeneous layers corresponding to the earth flattening transformation (approximately 0.001 km/s/km) raypaths corresponding to pure head wave propagation can be generated.

The ray tracing through the two-dimensional velocity structure provides travel time, distance, raypath parameter (slowness) and an amplitude factor for each seismic ray for input into the DRT synthesis program. The amplitude factor includes the amplitude effects of geometrical spreading, reflection and transmission coefficients at interfaces, a free-surface conversion factor and attenuation due to absorption. The attenuation is calculated from an exponential amplitude weighting factor ($\mathrm{Exp}(-\pi f \sum_{i=1}^{N} \frac{\Delta T_i}{Q_i})$) according to the travel-time spent within each Q layer. The attenuation due to absorption is approximated by this exponential absorption factor corresonding to the dominant frequency of the wavelet which will be used for the synthetic seismogram generation. Thus, it is a 'single frequency Q' approximation, and results in attenuation of the amplitude of propagated waves, but does not result in frequency dependent changes in waveform.

A flow chart shown in Figure 1 and a schematic diagram shown in Figure 2 illustrate the process of ray tracing and DRT seismogram synthesis

for a two-dimensional velocity model. Ray tracing through the velocity structure provides time, distance, raypath parameter and amplitude factors ($t_i$, $x_i$, $p_i$ and $a_i$) which can be used to generate a travel time curve for all of the phases of interest which are included in the ray tracing. DRT synthesis sums the contributions of individual amplitudes for raypaths in the vicinity of the desired seismogram location for all branches of the travel time curve and finally convolves the amplitude time series with a desired wavelet to produce individual seismograms. Repeating the amplitude summation for all distances of interest produces the seismic record section. The diagram shown in Figure 2 illustrates this process for a single seismogram at a distance $x_0$. In order to synthesize this seismogram by the DRT method, the time, distance, amplitude and raypath parameter values for the individual raypaths are generated by ray tracing through the velocity model. For each seismic phase (branch of the T-X curve), the amplitude contributions of individual raypaths are projected from their arrival time (using the slope equal to the raypath parameter) to the distance corresponding to the seismogram location $x_0$. Thus, seismic energy corresponding to raypaths arriving in the vicinity of the distance $x_0$ contribute to the amplitude of the arrival at the distance $x_0$. Distance and time weighting factors are utilized to prevent strong arrivals from large distances far away from the seismogram location being projected into the seismogram and contributing fictitious amplitude. Although the distance and time weighting factors are chosen arbitrarily, we have found that the process is not very sensitive to the choice of these weighting factors. The distance factor that we use generally corresponds to about 2 to 4 seismic wavelengths and the time window is approximately one period of the dominant frequency of the wavelet. After the individual amplitude contributions of each raypath are considered for each of the possible branches of the travel time curve within the distance given by the distance

weighting window, the individual time versus amplitude spikes are convolved with the wavelet to produce the DRT synthetic seismogram.

## MODEL STUDIES

In order to test the DRT method, the vertical component displacement theoretical seismograms (Figure 3) were computed at the surface of a model consisting of a homogeneous layer over a half space for an explosive point source at a depth close to the surface. The result is compared with modified reflectivity method (MRM) given by Kind (1978).

The velocity depth model was chosen arbitrarily for convenience so that all the major arrivals could be separated clearly. For the MRM seismograms, shear wave velocities and densities for layers of the model were computed from the P-wave velocities assuming a Poisson's ratio $\sigma = 0.25$. Densities were computed from $\rho_i = 0.252 + 0.3788\ \alpha_i$ (Birch, 1964). The effects of attenuation on body waves is included by introducing complex velocities (Braile, 1977).

For the DRT method, the $Q^{-1}$ factor which is dependent on a single predominant frequency, surface conversion coefficients (Cerveny and Ravindra, 1971), geometrical spreading, and reflection and transmission coefficients were taken into account in the amplitude calculation. For simplicity, only direct waves and primary P wave reflections with corresponding head waves are considered in the DRT seismograms. Later arrivals including multiple reflections are identified on the record section for the MRM seismograms. Amplitudes of both the DRT and MRM seismograms were multiplied by distance for convenient plot scaling.

Figure 3 shows theoretical seismograms computed by both the MRM and the DRT methods. The structure is a homogeneous layer over a half space with only the earth flattening transformation applied. For this case, ray-theoretical methods generally fails to predict the head waves,

but in our DRT computation, the head wave can be predicted and the relative amplitude and waveform character agree with the theoretical seismograms computed by the MRM. The major difference is in the critical point region (near 10 km) where the amplitude for the DRT method is larger than for the MRM, and the phase is distorted. This is due to the fact that wave theory predicts that the phase change due to reflection varies gradually in the near-critical region, whereas ray theory predicts that the phase shift for reflections begin abruptly at the critical distance. Although minor differences are apparent, comparison of the amplitude and waveform characteristics for the DRT and MRM synthetic seismograms shown in Figure 3 indicates that the DRT method is capable of accurate and efficient synthetic seismogram calculations.

## APPLICATION TO MODELING OBSERVED SEISMIC RECORD SECTIONS FROM THE SNAKE RIVER PLAIN AREA

Sparlin et al. (1982) have interpreted a 136 km reversed seismic line in the eastern Snake River Plain, Idaho (SP 7 SE in the northern Rocky Mountains province to the Gay Mine shotpoint located in the Basin and Range province) using ray-trace travel-time modeling. The velocity structure determined by Sparlin et al. (1982) is shown in Figure 4 along with the raypaths of principal refracted and reflected phases.

In this section, we compute the corresponding synthetic seismograms for the Sparlin et al. (1982) model and our modified model using DRT for the shotpoints (SP 7 SE and Gay Mine) at the ends of the velocity model. Observed and synthetic (DRT) record sections for the Snake River Plain model are shown in Figures 5 and 6. The synthetic seismograms calculated for the model proposed by Sparlin et al. (1982) based on travel-time modeling (Figure 4) display amplitude characteristics for phase E (Figures 4, 5 and 6) which do not match the observed data. A small

modification to the Snake River Plain velocity model (Figure 7) results in synthetic seismograms which match very closely the amplitude and even waveform character of the observed data for both the SP 7 SE (Figure 5) and Gay Mine (Figure 6) shotpoints. For example, the A, B, C phases (Figure 5) show the expected travel time delay due to block faulting. Large amplitude arrivals are calculated near 65 km in the D phase and from 60 to 110 km for the F phase (Figure 5). The very weak amplitude of phase E is seen on the synthetics for the modified model as observed on the real data.

In order to illustrate the importance of two-dimensional synthetic seismogram modeling such as for the Snake River Plain example (Figures 5 and 6), we computed MRM synthetic seismograms for a plane-layered model (laterally homogeneous) which approximately fits the travel times of th observed SP 7 SE and Gay Mine data. Although the arrival times match reasonably well, the amplitude and waveform character of these synthetics (Figure 8) display a poor comparison to the observed SP 7 SE and Gay Mine record sections. The excellent match of the two-dimensional DRT synthetics with the observed data and the inability to fit the observed data with a laterally homogeneous model provides confirmation of the complex velocity model beneath the eastern Snake River Plain. Additionally, this example illustrates the importance of amplitude data and synthetic seismogram modeling for detailed and accurate interpretation of crustal velocity structure.

## DISCUSSION AND CONCLUSIONS

Comparison of the synthetic seismograms computed with the DRT method with those of the reflectivity method have shown that the DRT method is efficient and reasonably accurate. The method can be applied to complex two-dimensional velocity and Q structures. Application to modeling

observed seismic refraction data for the eastern Snake River Plain has illustrated the significance of two-dimensional synthetic seismogram techniques and the utility of the DRT method. Modern refraction/wide-angle reflection data for crustal seismic studies will necessitate increased use of modeling techniques capable of laterally inhomogeneous velocity structure. Although the DRT method is an approximate technique and is some what restricted in its application, its efficiency and accuracy make it suitable for routine modeling of data in laterally inhomogeneous applications. The principal limitation that we have found with the DRT technique is the inability to trace rays through some complex geologic structures. This restriction is more a limitation of the ray tracing method than of the DRT seismogram synthesis.

## ACKNOWLEDGEMENTS

This research was supported by contracts from No. N00014-75-C-0972 and No. N00014-82-K-0033 from the Earth Physics Program, Office of Naval Research, and by U.S. Geological Survey Geothermal Research Program Grant No. 14-08-0001-G0674. We are grateful to Rainer Kind for providing a copy of his modified reflectivity program, Mark Odegard for helpful discussions and for a copy of his ray tracing and synthetic seismogram programs, and Walter Mooney and George McMechan for supplying the ray tracing program which was used in the DRT calculations.

# REFERENCES


Aki, K.E. and P.G. Richards, 1980, Quantitative Seismology - Theory and Methods, Volumes I and II, Freeman, San Francisco, 932 pp.

Alford, R.M., K.R. Kelly and D.M. Boore, 1974, Accuracy of finite-difference modeling of the acoustic wave equation, Geophysics, 39, 834-842.

Birch, F., 1964, Density and composition of the mantle and core, J. Geophys. Res., 69, 4377-4387.

Boore, D.M., 1972, Finite-difference methods for seismic wave propagation in heterogeneous materials, in Seismology: Surface Waves and Earth Oscillations (Methods in Computational Physics, Vol. 11), B.A. Bolt (ed.), Academic Press, New York.

Braile, L.W., 1977, Interpretation of crustal velocity gradients and Q structure using amplitude-corrected seismic refraction profiles, Geophysical Monograph 20, American Geophysical Union, 427-439.

Braile, L.W., R.B. Smith, J. Ansorge, M.R. Baker, M.A. Sparlin, C. Prodehl, M.M. Schilly, J.H. Healy, St. Mueller, and K.H. Olsen, 1982, The Yellowstone-Snake River Plain seismic profiling experiment: crustal structure of the eastern Snake River Plain, J. Geophys. Res., 87, 2597-2609.

Cerveny, V. and R. Ravindra, 1971, Theory of Seismic Head Waves, University of Toronto Press, Toronto, Canada, 312 pp.

Cerveny, V., I.A. Molotkov and I. Psencik, 1977, Ray Method in Seismology, Univerzita Karlova, Praha, 214 pp.

Cerveny, V., 1979, Ray theoretical seismograms for laterally inhomogeneous structures, J. Geophys., 46, 335-342.

Chapman, C.H., 1976, A first-motion alternative to geometrical ray theory, Geophys. Res. Lett., 3, 153-156.

Frazer, L.N. and R.A. Phinney, 1980, The theory of finite frequency body wave synthetic seismograms in inhomogeneous elastic media, Geophys. J.R. Astr. Soc., 63, 691-717.

Hong, T.L. and D.V. Helmberger, 1978, Glorified optics and wave propagation in non-planar structure, Bull. Seis. Soc. Amer., 68, 1313-1358.

Kelly, K., R. Ward, S. Treitel and R. Alford, 1976, Synthetic seismograms: a finite-difference approach, Geophysics, 41, 2-27.

Kind, R., 1978, The reflectivity method for a buried source, J. Geophys., 44, 603-612.

McMechan, G.A. and W.D. Mooney, 1980, Asymptotic ray theory and synthetic seismograms for laterally varying structures: theory and application to the Imperial Valley, California, Bull. Seis. Soc. Amer., 70, 2021-2035.

Smith, W.D., 1975, The application of finite element analysis to body wave propagation problems, Geophys. J.R. Astr. Soc., 42, 747-768.

Sparlin, M.A., L.W. Braile and R.B. Smith, 1982, Crustal structure of the eastern Snake River Plain determined from ray trace modeling of seismic refraction data, J. Geophys. Res., 87, 2619-2633.

Wiggins, R.A. and M.A. Madrid, 1974, Body wave amplitude calculations, Geophys. J.R. Astr. Soc., 37, 423-433.

Wiggins, R.A., 1976, Body wave amplitude calculation-II, Geophys. J.R. Astr. Soc., 46, 1-10.

# FIGURE CAPTIONS

Figure 1. Flow chart illustrating the process of calculation of synthetic seismograms by the disk-ray theory method.

Figure 2. Schematic diagram illustrating the calculation of synthetic seismograms by the disk-ray theory method. Upper diagram shows a travel time curve with a seismogram synthesized at the distance $x_0$. Middle diagram illustrates the velocity model with compressional wave velocities ($\alpha$) and attenuation factors (Q) described by a two-dimensional model including non-planar interfaces. Raypaths for direct, reflected and refracted waves through the velocity model are illustrated. Lower diagram illustrates the process of DRT amplitude synthesis in which the amplitudes for rays for a given travel time branch are added by projecting their time of arrival along the travel time curve and applying both distance and time weighting factors to the amplitude contributions of each raypath. The response at the distance $x_0$ is the sum of the weighted responses of each raypath for each travel-time branch projected to the appropriated arrival time. Convolution of the individual projected ray amplitudes with a source wavelet completes the disk ray theory seismogram synthesis.

Figure 3. Synthetic seismogram record section calculated using the modified reflectivity method (MRM) and disk ray theory (DRT) method for a plane homogeneous layer overlying a half-space. The single layer is 5 km thick with a velocity of 4.5 km/s overlying a half-space of velocity 6.8 km/s. Q values are 150 and 500 for the layer and half-space respectively. The DRT seismograms are displaced slightly to the left of the correct distance in the plot for clarity. The ray diagrams at the bottom of the figure illustrates the notation for the travel time branches.

Figure 4. Crustal model interpreted by Sparlin et al. (1982) for the eastern Snake River Plain in Idaho. The raypaths for a variety of refracted (upper diagram) and reflected (lower diagram) phases are shown. Numbers are compressional wave velocities in km/s. The datum is 1.2 km elevation. The location of shotpoint 7 and the Gay Mine shotpoint are at the northwest and southeast ends of the model, respectively. NRM is northern Rocky Mountains province; SRP is the Snake River Plain province; and BR is the Basin and Range province.

Figure 5. Observed and synthetic seismograms for the SP 7 SE profile across the velocity structure shown in Figure 4. Upper diagram shows the synthetic seismograms calculated by the DRT method for the Sparlin et al. (1982) model (Figure 4). Middle diagram illustrates the amplitude-corrected observed data for the SP 7 SE profile recorded during the Y-SRP 1978 experiment. Lower diagram shows the synthetic seismograms calculated by the DRT method for the modified SP 7 SE model (Figure 7). The amplitudes for all of the seismograms shown in this figure are scaled with a distance factor of amplitudes times distance to the 1.5 power for convenient amplitude scaling. The phase notation shown in the middle seismic section corresponds to the phases illustrated in Figure 4.

Figure 6. Observed and synthetic seismograms for the Gay Mine shotpoint (Figure 4). Upper diagram illustrates the synthetic seismograms calculated by the DRT method for the Gay Mine shotpoint and the velocity structure shown in Figure 4. Middle diagram shows observed data from the Gay Mine shotpoint. Lower diagram illustrates synthetic seismograms calculated by the DRT method for the modified Gay Mine model (Figure 7). All of the seismograms in these record sections have been scaled with the identical scaling factor of amplitude times distance to the 1.5 power to provide for convenient plot scaling.

Figure 7. Velocity structure for the modified eastern Snake River Plain model. The principal modification of this model as compared to the Sparlin et al. (1982) model illustrated in Figure 4 is a flattening of the interface separating the 6.53 km/s layer from the 6.15 km/s layer beneath the Snake River Plain (SRP). This modification to the velocity structure primarily affects calculation of the phase E (Figure 4) for which raypaths are illustrated. Numbers in parentheses are Q values used in the DRT calculations for the SP 7 SE and Gay Mine synthetic seismograms (Figures 5 and 6) and are based on the Q values interpreted by Braile et al. (1982).

Figure 8. Synthetic seismograms calculated by the modified reflectivity method for a plane layered structure whose travel times approximate the observed travel time data for the SP 7 SE and Gay Mine observed record sections. The velocity and Q structure are illustrated in the left hand diagram. Amplitudes of the seismograms are multiplied by distance to the 1.5 power for convenient plot scaling.

FLOWCHART FOR DISK RAY THEORY

SYNTHETIC SEISMOGRAM CALCULATION

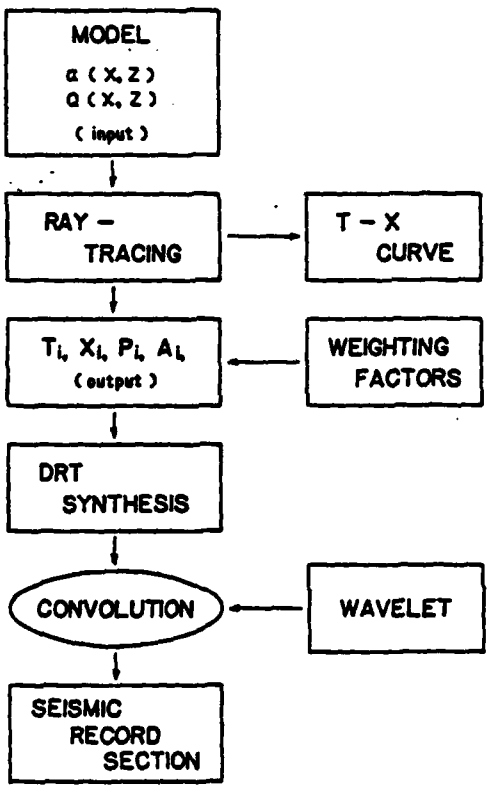


Figure 1

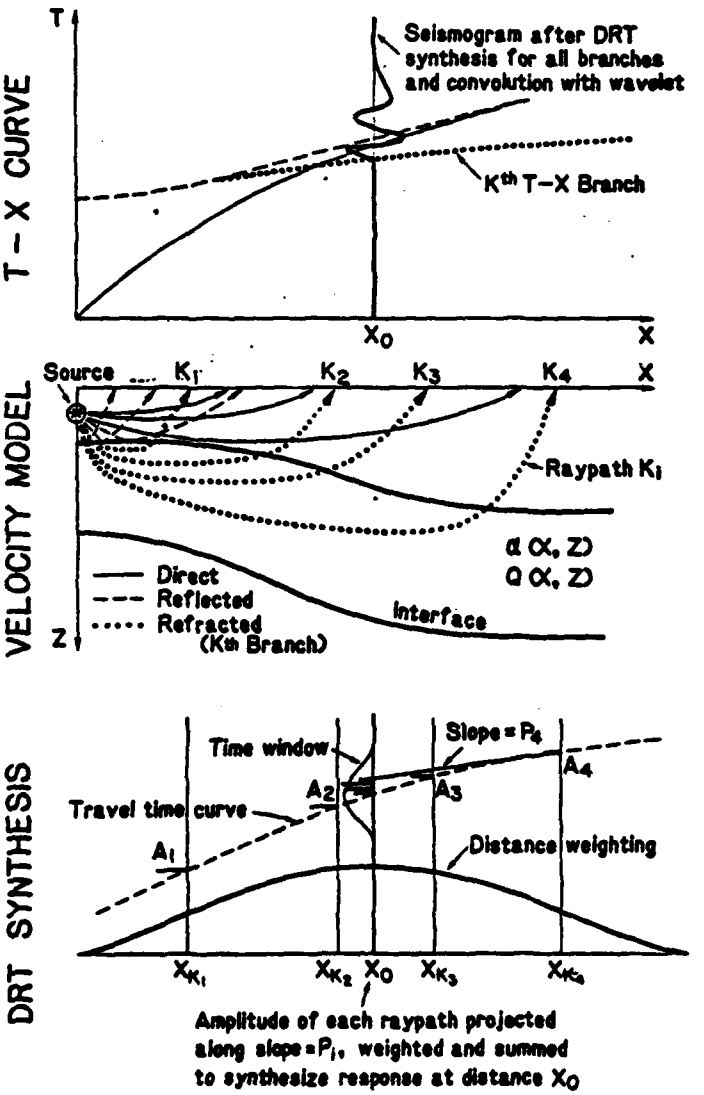
T - X CURVE
T
Seismogram after DRT synthesis for all branches and convolution with wavelet
K^th T-X Branch
X0
X
VELOCITY MODEL
Source
K1
K2
K3
K4
X
Raypath K1
α (X, Z)
Q (X, Z)
Direct
Reflected
Refracted (Kth Branch)
Interface
Z
DRT SYNTHESIS
Time window
Slope = P4
A4
A2
A3
Travel time curve
A1
Distance weighting
XK1
XK2
X0
XK3
XK4
Amplitude of each raypath projected along slope = Pi, weighted and summed to synthesize response at distance X0

Figure 2

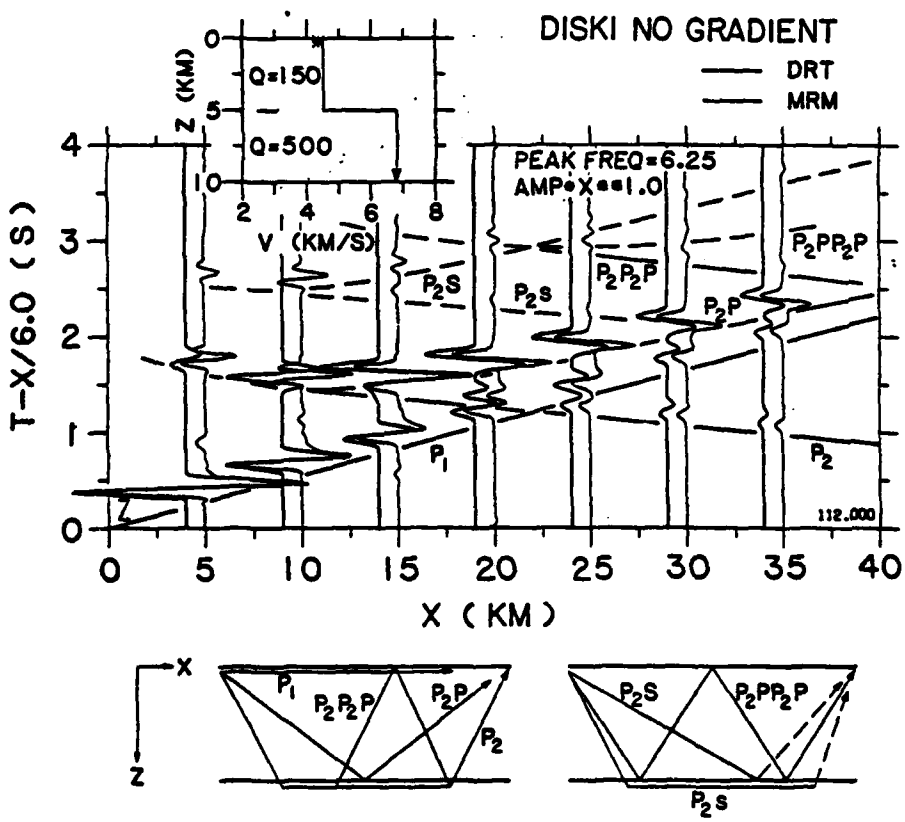
DISKI NO GRADIENT
DRT
MRM
Z (KM)
Q=150
Q=500
V (KM/S)
PEAK FREQ=6.25
AMP•X••1.0
T-X/6.0 (S)
X (KM)
P1
P2S
P2P2P
P2PP2P
P2P
P2
P2s
112.000
X
Z

Figure 3

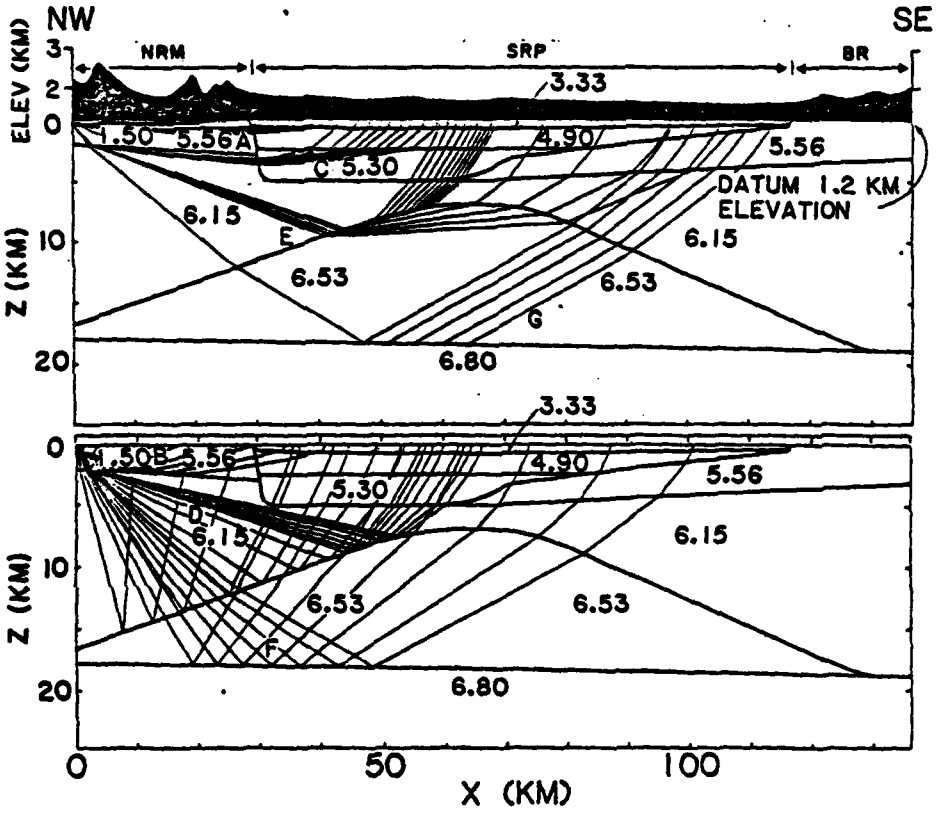
NW
SE
NRM
SRP
BR
ELEV (KM)
3
2
0
3.33
1.50
5.56A
4.90
5.56
C
5.30
DATUM 1.2 KM
ELEVATION
6.15
E
6.15
10
Z (KM)
6.53
6.53
G
20
6.80
3.33
0
1.50B
5.56
4.90
5.56
5.30
D
6.15
6.15
10
Z (KM)
6.53
6.53
F
20
6.80
0
50
100
X (KM)

Figure 4

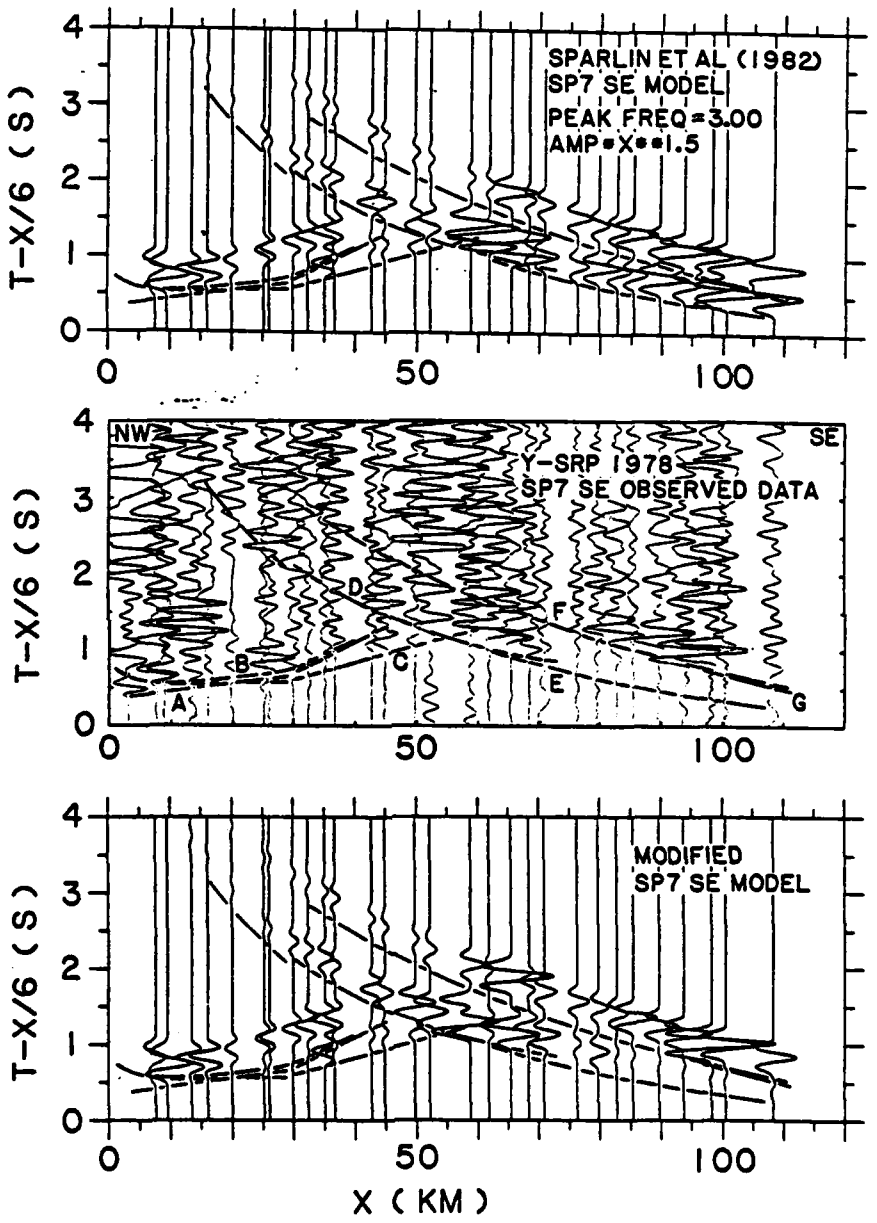
SPARLIN ET AL (1982)
SP7 SE MODEL
PEAK FREQ=3.00
AMP=X**1.5
T-X/6 (S)
NW
SE
Y-SRP 1978
SP7 SE OBSERVED DATA
A
B
C
D
E
F
G
MODIFIED
SP7 SE MODEL
X (KM)
0
50
100
1
2
3
4

Figure 5

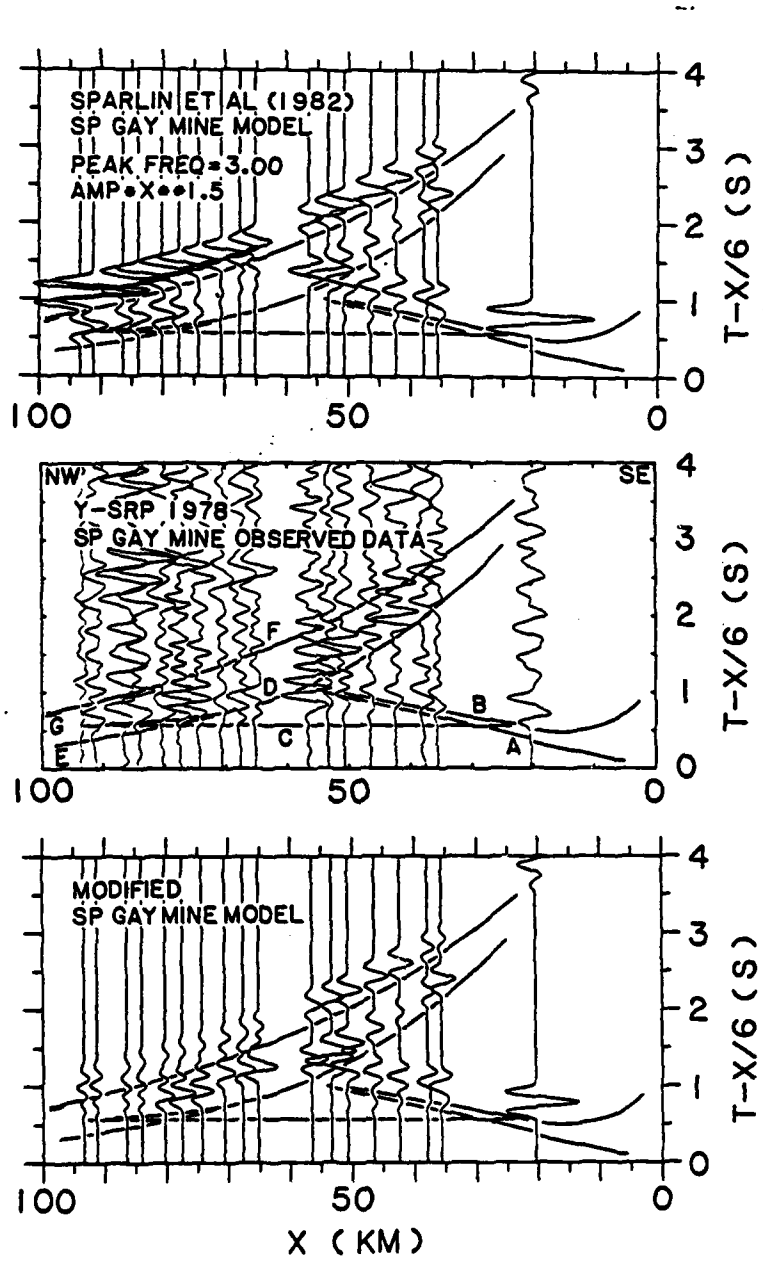
SPARLIN ET AL (1982)
SP GAY MINE MODEL
PEAK FREQ=3.00
AMP•X••1.5
NW
SE
Y-SRP 1978
SP GAY MINE OBSERVED DATA
A
B
C
D
E
F
G
MODIFIED
SP GAY MINE MODEL
100
50
0
X (KM)
T-X/6 (S)
0
1
2
3
4

Figure 6

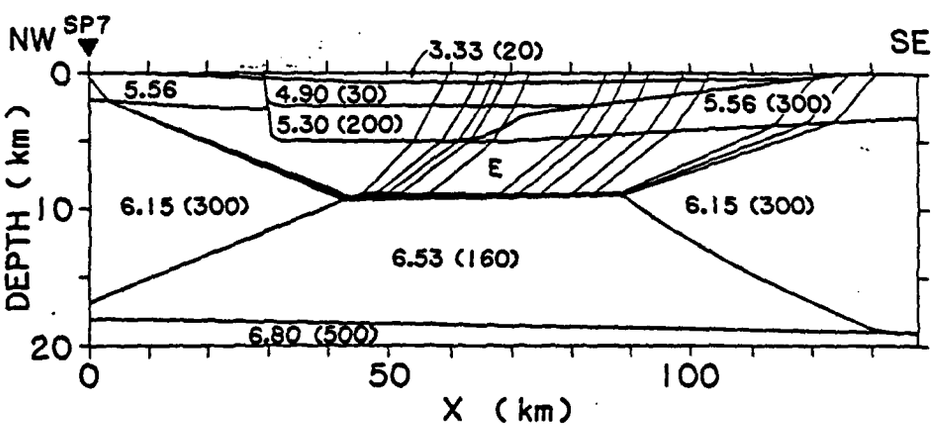
NW
SP7
SE
3.33 (20)
5.56
4.90 (30)
5.30 (200)
5.56 (300)
E
6.15 (300)
6.15 (300)
6.53 (160)
6.80 (500)
DEPTH (km)
0
10
20
0
50
100
X (km)

Figure 7

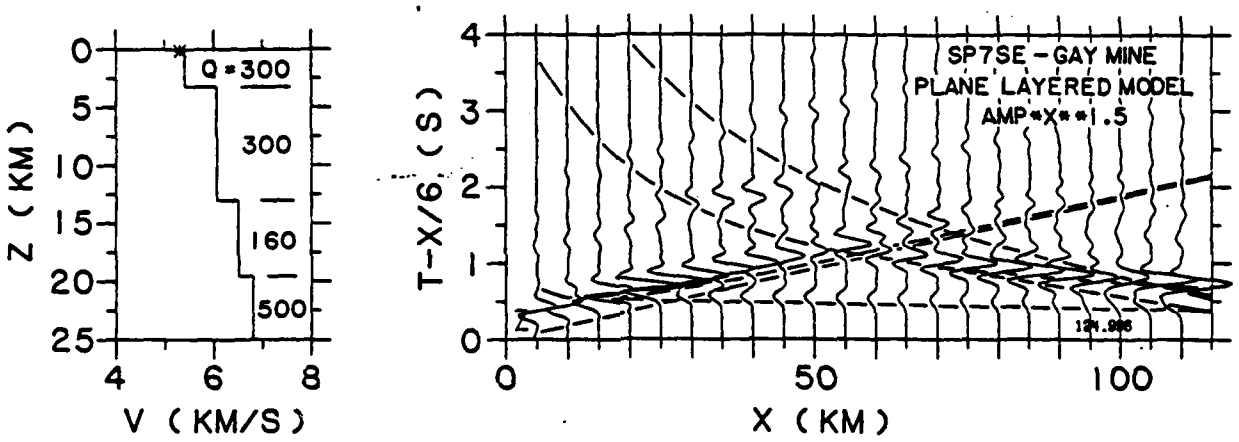
Z (KM)
0
5
10
15
20
25
Q=300
300
160
500
4
6
8
V (KM/S)
T-X/6 (S)
4
3
2
1
0
0
50
100
X (KM)
SP7SE - GAY MINE
PLANE LAYERED MODEL
AMP=X**1.5

Figure 8

END

FILMED

9-83

DTIC